Timing System Design for PNT Satellite Constellation: Time Scale Generation and Distributed Clock Synchronization

Ruiqi Li

A thesis
submitted in partial fulfillment of the
requirements for the degree of

Master of Science in Aeronautics and Astronautics

University of Washington

2026

Committee:

Mehran Mesbahi

Amir Taghvaei

Program Authorized to Offer Degree:
Aeronautics and Astronautics

University of Washington

Abstract

Timing System Design for PNT Satellite Constellation: Time Scale Generation and Distributed Clock Synchronization

Ruiqi Li

Chair of the Supervisory Committee:
Mehran Mesbahi
Aeronautics and Astronautics

Accurate positioning and time keeping are the most important services provided by the PNT satellite systems. In recent years, the need for higher accuracy positioning and time keeping, more extensive coverage, and better safety for the PNT satellites has increased. Designing new PNT satellite constellations to enhance or replace existing architectures has attracted significant interest. This research examines two key aspects of timing systems for PNT constellations: generating a stable time scale and clock synchronization between the satellites.

To generate a stable time scale, this research introduces a mixed clock ensemble algorithm and a linear quadratic Gaussian clock steering algorithm for its realization. This Kalman filter-based algorithm allows for the combination and enhancement of individual clocks' stability. Results indicate that the time scale generated by the algorithm yields better performance than any single clock in the group, and the capability of the control algorithm to achieve this time scale.

For clock synchronization, this work investigates two approaches. The first approach is to utilize the existing PNT constellation, such as GPS. An extended Kalman filter method is introduced to identify the clock bias between satellite time and GPS time. Simulation results demonstrate that the algorithm tracks the biases accurately. The second approach is using the consensus algorithm for synchronization. This method is based on the communication

between the satellites in the constellation, which provides robustness and less dependence on external sources. Numerical simulation shows that synchronization can be achieved quickly with the consensus algorithm.

TABLE OF CONTENTS

Page

List of Figures . . . iii

Glossary . . . iv

Chapter 1: Introduction . . . 1
- 1.1 Timing Systems in current PNT Satellite constellations and Challenges . . . 3
- 1.2 Thesis Contribution . . . 5
- 1.3 Thesis Structure . . . 5

Chapter 2: Theoretical Foundations . . . 7
- 2.1 Basic Concepts in Precise Time . . . 7
- 2.2 Linear Clock Model . . . 8
- 2.3 Allan Variance . . . 9
- 2.4 Kalman Filter and Extended Kalman Filter . . . 10
- 2.5 Two-Way Time Transfer . . . 11
- 2.6 Graph theory and consensus protocol . . . 13

Chapter 3: Mixed Clock Ensemble . . . 16
- 3.1 Implicit Ensemble Mean . . . 17
- 3.2 Steering OCXO for IEM Realization . . . 19
- 3.3 Simulation . . . 21
- 3.4 Discussion . . . 23

Chapter 4: Onboard Clock Synchronization via GNSS . . . 24
- 4.1 Global Navigation Satellite System . . . 25
- 4.2 Nonlinear Least Square . . . 26
- 4.3 Extended Kalman Filter . . . 28
- 4.4 Simulations . . . 29
- 4.5 Discussion . . . 30

Chapter 5: Time synchronization over Satellite Constellation via Inter-Satellite Links . . . 34
5.1 Synchronization using PI Consensus Algorithm . . . 34
5.2 Proof of Convergence . . . 36
5.3 Information Exchange Networks . . . 38
5.4 Simulations and Results . . . 39
5.5 Discussion . . . 41

Chapter 6: Conclusions . . . 45
6.1 Future Efforts . . . 47

Appendix A: GPS Satellite Geometry and Dilution of Precision . . . 54

Appendix B: Convergence of Consensus . . . 56

LIST OF FIGURES

Figure Number — Page

1.1 Satellite navigation concept illustration . . . 2
1.2 Two types of popular clocks . . . 4

2.1 Visualization of computation of Allan variance . . . 9
2.2 Visualization of two-way time transfer . . . 12
2.3 Undirected graph with 12 vertices and 14 edges . . . 15

3.1 Clock ensemble and realization[1] . . . 17
3.2 Clock ensemble with different settings . . . 22
3.3 Clock ensemble realization with different settings . . . 23

4.1 Visualization of the zenith angle . . . 26
4.2 Position estimation profile . . . 31
4.3 Bias estimation history for EKF and nonlinear least square . . . 31
4.4 Position estimation error history . . . 32
4.5 Bias estimation error history . . . 32

5.1 Satellite network with 500 satellites under different ISL ranges . . . 39
5.2 Satellite network with 900 satellites under different ISL ranges . . . 40
5.3 Consensus on 300 satellites for different ISL ranges . . . 41
5.4 Consensus on 500 satellites for different ISL ranges . . . 42
5.5 Average variance over time for different numbers of satellites and ISL range combination . . . 43

GLOSSARY

ALLAN VARIANCE: A metric to evaluate the frequency stability of an atomic clock, as well as other instruments like amplifiers and oscillators.

KALMAN FILTER: An optimal estimation algorithm using previous estimation and error covariance to perform state estimation recursively in real time.

EXTENDED KALMAN FILTER: The extended version of the Kalman filter handles nonlinear dynamics and nonlinear measurements.

ATOMIC CLOCK: A piece of equipment for measuring time through tracking the resonance of the atoms. Highly stable and accurate time measurement standard.

OVEN CONTROLLED CRYSTAL OSCILLATOR: A highly stable frequency standard that can be controlled by varying the temperature.

CLOCK COMPOSITE: A concept of combining multiple atomic clock sources to create a single stable timescale.

IMPLICIT ENSEMBLE MEAN: The realization of the clock composite. Computed through estimation of the clock states via the Kalman Filter.

CLOCK BIAS: Clock bias or clock drift stands for the difference between the local clock and the reference time scale.

FREQUENCY DRIFT: Drift of the oscillation frequency of oscillators.

PSEUDORANGE MEASUREMENT: The pseudo-distance between the GNSS satellite and the receiver contains the true distance, clock bias times speed of light, and other disturbance factors.

TIME TRANSFER: Technique of creating and distributing time scales to multiple sites that require a common time reference.

INTER-SATELLITE LINK: The communication link between satellites enables information exchange. Common media are laser and radio waves.

TIME SYNCHRONIZATION: A concept of coordinating the individual clocks to agree on a common clock reading.

CONSENSUS IN CONTROL: Protocol to drive agents with communication in a network to an agreed state or value.

TIME SCALE: A system of measuring time and assigning time stamps.

GLOBAL NAVIGATION SATELLITE SYSTEM (GNSS): A family of satellite constellations is specified for providing positioning, navigation, and timing services.

GLOBAL POSITIONING SYSTEM (GPS): The earliest GNSS system in the world, was developed by the United States.

ECEF FRAME: Earth-centered, Earth-fixed frame. A coordinate system with origin in the Earth's center of mass rotating with the Earth. Widely used in satellite motion and satellite navigation.

LINE OF SIGHT: A virtual line between the object of interest and the observer.

ELEVATON ANGLE: The angle between the horizontal line of sight and the line of sight to the object of interest.

LEAST SQUARE: A method to determine the best-fit polynomial or functions given a set of observations by minimizing the sum of squared residuals.

LEO SATELLITES: The satellites operate in low Earth Orbit, usually at an altitude between 160 km and 1000 km.

LQG CONTROL: Linear Quadratic Gaussian Control. An optimal control method dealing with a linear dynamical system with additive Gaussian noise.

PID CONTROL: A control strategy using proportional, Integral, and derivative of the distance between the current value and desire value to regulate the system.

ACKNOWLEDGMENTS

I would like to first express my deepest gratitude to my advisor, Professor Mehran Mesbahi, who led me into the academic research world. He always encourages me to explore my interests, pushing me to become a better person, and gives me timely and insightful guidance and advice when I feel lost or confused.

I would also like to thank Professor Amir Taghvaei for agreeing to be a member of my thesis committee. His guidance and encouragement helped me massively in my growth as a graduate student.

I would also like to deeply appreciate my lab mates at the RAIN lab for welcoming and accepting me as a member of the group. It is a great honor to be in such a creative, energetic, and collaborative group. The group meetings and conversations with them are always so interesting, educational, and incredibly enriching for me.

Last but not least, I would like to thank my beloved parents, Dajun and Xiuyi, and my grandparents Huohuan, Xuezhu, Yanhui, and Aiqin, and all of my family. Their unconditioned love and support have sustained me and brought me to where I am today.

DEDICATION

To my parents,

Dajun and Xiuyi

Chapter 1
INTRODUCTION

Precise timing and time synchronization serve as a crucial cornerstone of many aspects of human society. In positioning and navigation, the most popular approach nowadays is using the Global Navigation Satellite Systems (GNSS) [2, 3], which requires at least 4 satellites with accurate and synchronized clocks to pinpoint a receiver's position. Figure 1.1 [3] shows an illustration of this concept. For the financial markets, accurate time stamping is critical for tracking and maintaining the safety and fairness of each transaction, and synchronized time across different stock exchanges ensures the accurate execution of the transactions. For power utilities, synchronized time over the power grid enables the engineers to track the outage efficiently. The other scenarios that require accurate timing and synchronization are military, agriculture, transportation, and so on [4].

Since ancient times, people have been researching accurate timekeeping tools. The most famous examples are the water clock, or clepsydra, measuring the time using water flow, and the sundial using the projected shadow. These methods have been developed and have lots of variations over time. As humans developed the ability to send satellites into space, using the satellites for positioning, navigation, and timing (PNT) [5, 6] became one of the most important applications. The earliest satellite-based PNT system is the Global Positioning System, built by the United States starting in the 1970s. With a few decades of development, the GPS constellation is now constituted of 32 operational satellites. Most of the applications introduced above are synchronized to the GPS time. Meanwhile, the other countries or entities around the globe have developed their own Satellite PNT systems, such as GLONASS from Russia, Beidou from China, and Galileo from Europe. These satellite constellations form a family of PNT systems called the Global Navigation Systems. Using the satellite constellations for PNT provides significant advantages. First, the satellite constellations orbit around the Earth, which provides good coverage and enables navigation

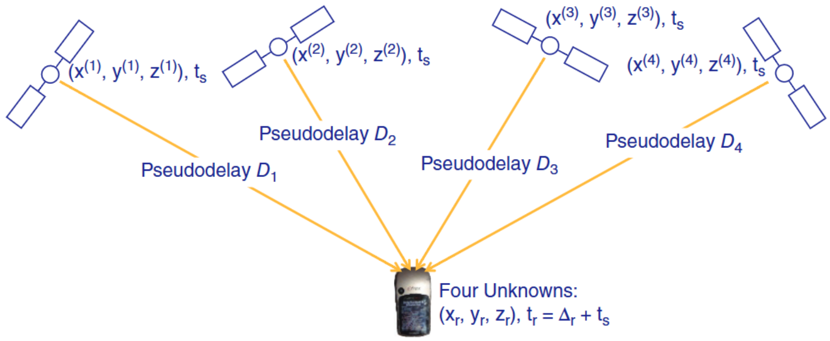

Figure 1.1: Satellite navigation concept illustration

and timing services around the globe. Second, the GNSS satellites are all equipped with high-precision, ultra-stable atomic clocks and synchronized with the common time scale that is being used widely, which is the universal coordinated time (UTC) [7]. Last but not least, the service provided by the GNSS is always consistent as they keep operating.

However, with increasing demands for precision, security, and service coverage—coupled with the emergence of new technologies such as inter-satellite links—research into next-generation PNT satellite constellations is becoming a focal point within the space community. This paper aims to investigate two aspects of the design of PNT constellation time systems. The first is the generation of time scales. Time scale is a system of assigning timestamps to events [8]; its stability and consistency are critical for accurate time measurements. This work introduced a mixed clock ensemble method for generating stable time scales. The second aspect being investigated is the synchronization of the clocks over the PNT satellite constellation. The synchronization problem aims to drive all the clocks in the satellite constellation to agree with each other, which is critical in navigation applications. In this work, two approaches for clock synchronization are presented, with one aimed at synchronizing the PNT satellite with the current GNSS systems, such as GPS, and the other approach is based on graph theory and consensus protocol, aiming to achieve synchronization within the constellation.

1.1 *Timing Systems in current PNT Satellite constellations and Challenges*

The current GNSS constellations are usually equipped with multiple high-precision and high-stability atomic clocks. For example, the GPS satellites are equipped with Rubidium atomic clocks [9], which are small in size and drift only a few nanoseconds (10^{-9}) every day. The bias of the clocks on the satellite is monitored and calibrated by the ground stations periodically, where the ground stations are equipped with ultra-stable Hydrogen master clocks. The GPS time is the time scale operated by the GPS. It is given by the composite clock, which consists of all the clocks on the GPS satellites and the ground stations around the world. The GPS time is highly related to the current primary time standard: Universal Coordinated Time (UTC), which is ahead of the UTC by 18 seconds. This gap is also called the leap second.

Due to the increasing number of users and corresponding regulatory and performance requirements, the timing systems and the PNT constellations are facing more and more challenges. First, despite the clocks onboard the GNSS satellites being of high quality, as time goes by, the drift and aging of these clocks are inevitable. This will significantly degrade the performance of the timing service provided by the GPS systems. In addition, the current GNSSs operate in the medium Earth orbit (MEO), which adds more disturbances and latencies to the signals from the PNT satellites for timing and navigation.

The emerging alternative or enhancement for the current GNSS is using mega-constellations that operate in low Earth orbit (LEO) [10, 11, 12], such as Starlink from SpaceX or Kuiper from Amazon. This routine is meant to exploit the coverage and robustness of the mega-constellations, but also imposes challenges in the timing system design. The first is the price. The Rubidium atomic clocks on the GNSS right now are stable. However, they are at a very high price. For LEO mega-constellations with a high number of satellites, it is impossible to equip all of them with clocks of the same quality. Therefore, the clocks at lower prices as substitutes are necessary. The lower-priced clocks usually face the problem of instability in frequency, are prone to drifting, and are impacted by temperature and other factors in the space more severely than the atomic clocks. Generating a stable and consistent time scale in these scenarios will be difficult. The other challenge is synchronization. To encounter the bias accumulation over time, the transitional GNSS systems rely on the monitoring and correction from a large ground control network around the globe. This approach is not sustainable when the PNT constellations have a large number of satellites, as it requires much more computation and energy to keep track of each one of them. More autonomous ways of synchronizing the clocks over the constellation are needed.

Outside the use cases on Earth, as space exploration missions are increasing, especially the missions with crew in the future, such as Lunar and Mars exploration, higher accuracy PNT systems specialized for these missions to improve mission coordination, scheduling, and navigation are in demand. The primary challenge imposed in designing these PNT systems is that they are all far away from the Earth. Performing synchronization from the ground will be challenging. The more feasible approach is to synchronize the PNT constellation with the GNSS or to do synchronization autonomously within the constellation itself. The second is the relativistic effect. As the gravitational field distribution and orbiting speed for the satellites around these celestial bodies differ from those of the Earth, the relativistic effect will cause time scale inconsistency, which leads to the problem of stable and consistent time scale generation.

(a) Rubidium atomic clock

(b) Oven Controlled Quartz Oscillator

Figure 1.2: Two types of popular clocks

1.2 Thesis Contribution

The mixed clock ensembles algorithm and its realization, introduced in this work, enable a more robust time scale generation over a group of different types of clocks. This algorithm computes the composite clock by estimating each clock's bias through a Kalman filter; a single clock's failure or adding a new clock will not affect the stability of the composite clock. If all clocks are of the same type, the stability of the ensemble time scale improves by a factor of N compared to that of an individual clock. This is useful for megaconstellations, even if each satellite is only equipped with lower-stability clocks. In addition, the mixed clock ensemble algorithm combines the advantages of different clock types; therefore, in a heterogeneous setting, it can achieve both long-term and short-term stability simultaneously. This provides more design space for clock selection in future time system designs.

Research on synchronizing the satellite clock with the current GNSS time provides consistency between the new PNT constellation and the existing PNT architecture, as well as with the world's popular time standard. In addition, receiving GNSS signals from space has the advantage of lower signal degradation and multipath effects. With the reference from the current GNSS, the need for a large ground station for tracking will be reduced, enabling the new PNT constellation to operate more autonomously.

On the other hand, synchronization using the consensus algorithm aims to increase the robustness of the clock networks formed by the satellites and decrease the reliance on external sources. With the use of Inter-satellite links, the satellites within the constellation are capable of communicating with each other, which lays the foundation of synchronization. The consensus introduced in this work uses minimum information from the other satellites, which is the clock reading difference, and can be achieved by two-way time transfer using the ISL very quickly. The convergence criteria for satellite constellation design are also investigated through simulation.

1.3 Thesis Structure

This section presents the structure of this thesis, with a summary of the topics and contents for each chapter. Chapter 1 discusses the motivations and applications for an accurate space-based timing system, problems of concern, prior works, and proposed solutions.

In Chapter 2, the mathematical fundamentals for this work are presented, including some of the basic concepts in time, the linear clock model, the Kalman Filter, Allan variance, two-way time transfer, and some basic graph theory and consensus protocols.

In Chapter 3, the concept of a mixed clock ensemble is presented. This technique is aimed at generating a time scale with robustness and long-term stability. First, the Kalman filter-based algorithm to compute the clock ensemble is introduced. Then, the second Kalman filter was used to steer the controlled clock to achieve the ensemble. Finally, the numerical simulation results are presented.

Chapter 4 introduced clock synchronization using measurements from the current Global Navigation Satellite Systems (GNSS). This chapter aims to explore synchronizing the PNT constellations with the current GNSSs, which ensures consistency with the current standard time scale in the world. Two methods, Nonlinear least squares and Extended Kalman Filter, are presented. The parameters for the Extended Kalman filter are reported. The setup for a simulation and its result are also presented in this chapter. The chapter ended with a discussion on the simulation results for both methods and possible future research directions down this avenue.

Chapter 5 discusses using the consensus algorithm to achieve clock synchronization within the satellite constellation with the use of an inter-satellite link. This method aims to enhance the robustness and decrease the dependency on external sources for time synchronization. The effectiveness of the algorithms is demonstrated through simulations. Following a discussion on the underlying network architecture formed by the satellites.

Finally, Chapter 6 summarizes the findings and problems that emerged from this work. Some possible future research questions in this field are also proposed.

Chapter 2
THEORETICAL FOUNDATIONS

In this chapter, we discuss the mathematical fundamentals used in different sections of this thesis. We begin by introducing some basic concepts in precise time to build up intuition and motivation. Then, the clock models and dynamics, followed by Allan variance, which is the metric to evaluate its stability, are presented. The two-way time transfer for determining the clock difference is also introduced. Next, the Kalman filter and extended Kalman filter for state estimation are presented. Finally, some fundamental graph theory concepts and the consensus protocol are presented to lay the foundation for synchronization over the satellite network.

2.1 Basic Concepts in Precise Time

Time scale The time scale, sometimes also called time standard in the PNT field, is a system of timekeeping and assigning timestamps, such as date or epoch. The earliest time scale is the apparent solar time, which uses the apparent motion of the sun to define a "day". In precise time measurement and PNT literature, the atomic clocks are used to generate smaller and more precise time scales, such as seconds or microseconds. However, just as there are no two rulers in the world that can give exact centimeter measures, none of the clocks in the world can define a second exactly in the same way. Therefore, a universally agreed-upon time scale is needed for people around the world to agree on and coordinate on top of it. The most popular time scale nowadays is the Coordinated Universal Time (UTC) [13]. The UTC consists of hundreds of free-running atomic clocks across the globe and combines them through an algorithm.

Date and Time Interval The date and time interval are the two meanings that people usually refer to as "time". The date or datetime is a timestamp for an event. An example of a date is 4/20/2026, 00h, 00m, 00s, where **h, m, s** stands for hours, minutes, and seconds.

To assign a date, an agreed beginning and a time scale for counting are required. The time interval, on the other hand, refers to the length or duration of time between two events. The measure of time interval only relies on a clock or counter.

2.2 Linear Clock Model

This work uses a two-state clock model to describe the atomic clocks [14, 15]. In the precision time-keeping community, such as GNSS, atomic clocks are the most widely used family of devices. Time measurement using atomic clocks is performed by monitoring the cycles of a resonant signal in the atoms [16, 17]. These clocks can be modeled as a non-ideal oscillator:

$$u(t) = U_0 \sin(2\pi v_0 t + \phi(t)), \tag{2.1}$$

where U_0 is the amplitude, v_0 is the nominal frequency, and $\phi(t)$ is the time-varying phase. Defining the true time as $h_0(t) = t$, then the clock reading is $h(t) = h_0(t) + \frac{\phi(t)}{2\pi v_0} = t + \frac{\phi(t)}{2\pi v_0}$. The phase offset is defined as $x(t) = \frac{\phi(t)}{2\pi v_0}$. Note that as the true time t is unknown, hence $x(t)$ is unobservable. We also defined the instaneous frequency as $\nu(t) = \nu_0 + \frac{1}{2\pi}\frac{d\phi(t)}{dt}$, and its normalized version

$$y(t) = \frac{\nu(t) - \nu_0}{\nu_0}, \tag{2.2}$$

where $y(t)$ is the frequency offset. It can also be realized that $\frac{dx(t)}{dt} = y(t)$.

The dynamic model of a clock is then defined as

$$\begin{bmatrix} \frac{dx(t)}{dt} \\ \frac{dy(t)}{dt} \end{bmatrix} = \begin{bmatrix} 0 & 1 \\ 0 & 0 \end{bmatrix} \begin{bmatrix} x(t) \\ y(t) \end{bmatrix} + w. \tag{2.3}$$

where w is the process noise vector. Throughout this work, the discretized version of this model is utilized

$$\begin{bmatrix} x(t_{k+1}) \\ y(t_{k+1}) \end{bmatrix} = \begin{bmatrix} 1 & \tau \\ 0 & 1 \end{bmatrix} \begin{bmatrix} x(t_k) \\ y(t_k) \end{bmatrix} + w, \tag{2.4}$$

where τ is the discretization step size.

The process noise vector w is drawn from distribution $\mathcal{N}(0, Q(\tau, \sigma_1^2, \sigma_2^2))$, the Q matrix is constructed as

$$Q(\tau, \sigma_1^2, \sigma_2^2) = \begin{bmatrix} \sigma_1^2 \tau + \sigma_2^2 \frac{\tau^2}{3} & \sigma_2^2 \frac{\tau^2}{2} \\ \sigma_2^2 \frac{\tau^2}{2} & \sigma_2^2 \tau \end{bmatrix}, \tag{2.5}$$

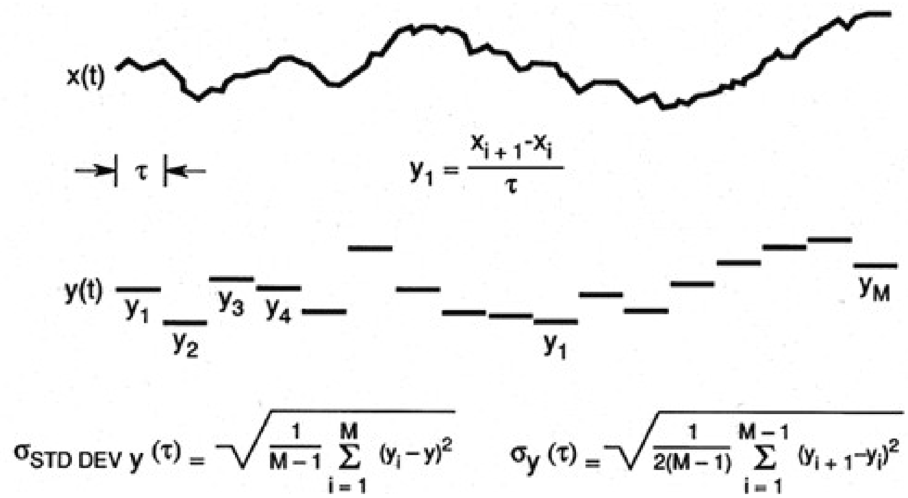

Figure 2.1: Visualization of computation of Allan variance

where σ_1^2 and σ_2^2 are the parameters that vary for different types of clocks. In practice, these parameters are determined by computing the Allan variance of the drift of the clocks over time [15].

2.3 Allan Variance

The Allan variance is a tool for analyzing the frequency stability and identifying noise types for atomic clocks [18, 19, 20]. For atomic clocks, the Allan variance can identify five types of noise: white phase noise, white frequency noise, flicker phase noise, flicker frequency noise, and random-walk frequency noise.

Here we present the computation of the Allan variance. The visualization of this computation is shown in Figure 2.1. Given a time series of data $x(t)$, first define

$$\bar{y}_i = \frac{x(iT + \tau) - x(iT)}{\tau}, \quad i = 0, 1, \ldots \tag{2.6}$$

where T is the time between each sample and τ is the observation interval. The Allan variance is defined as

$$\sigma_y^2(\tau) = \frac{1}{2(M-1)}\sum_{i=1}^{M}(\bar{y}_{i+1} - \bar{y}_i)^2 \tag{2.7}$$

where M stands for the number of fractions of the data divided by τ. In plain words, the Allan variance is computed by dividing the time-series data into intervals with width τ, taking the average over intervals, then calculating the square of differences between the average of consecutive intervals, and finally computing the average of them and dividing by 2. Similar to variance and deviation, the Allan deviation is defined as

$$\sigma_y(\tau) = \sqrt{\sigma_y^2(\tau)}. \tag{2.8}$$

The Allan variance is interpreted through plotting σ_y^2 as a function of τ, the plot is in log-log scale. In general, lower Allan variance indicates better frequency stability. In addition to atomic clocks, the Allan variance can also be used to characterize the stability of other sensors, such as gyroscopes and accelerometers.

2.4 Kalman Filter and Extended Kalman Filter

The Kalman Filter is the most popular tool for state estimation of linear dynamical systems [21], and it has a wide application in navigation, aerospace, and many other fields [22, 23, 24]. In this work, the Kalman filter is used to estimate clock states [25]. Here we present the Kalman filter algorithm in a discrete-time setting. Denote x_k and $\hat{x}_k$ as the true state and its estimate at time step k. The Kalman filter requires the previous estimate $\hat{x}_{k-1}$, previous estimate covaraince $\hat{P}_{k-1}$, current measurement z_k as input, and outputs the current estimate $\hat{x}_k$ and current estimate covariance $\hat{P}_k$. The discrete-time linear dynamic model is described as

$$x_{k+1} = Ax_k + Bu_k + w_k \tag{2.9}$$

where A is the state transition matrix, u_k is the control input at k, B is the control mapping, and w is the process noise vector associated with a zero-mean Gaussian noise with covariance matrix Q. The measurement z_k is also obtained through a linear model

$$z_k = Hx_k + v_k \tag{2.10}$$

where H is the observation matrix and v_k is measurement noise drawn from a Gaussian distribution with zero mean and covariance matrix R.

The Kalman Filter contains two steps: predict and update. The predict stage propagates the estimated state and covariance from the last time steps, and the update stage corrects the prediction using the measurement at the current time step. The Kalman filter algorithm is summarized below:

$$\text{predict} \quad \begin{cases} \bar{x}_k = A\hat{x}_{k-1} + Bu_k \\ \bar{P}_k = A\hat{P}_{k-1}A^T + Q \end{cases} \tag{2.11}$$

$$\text{update} \quad \begin{cases} K_k = \bar{P}_k H^T (H\bar{P}_k H^T + R)^{-1} \\ \hat{x}_k = \bar{x}_k + K_k(z_k - H\bar{x}_k) \\ \hat{P}_k = (I - KH)\bar{P}_k \end{cases} \tag{2.12}$$

The matrix K_k is the Kalman gain.

In the case where the dynamical system and measurement are nonlinear, which is true in most of the engineering applications, the Extended Kalman filter (EKF) [23] can be used. Denote the discrete-time nonlinear dynamical model and measurement model as $x_{k+1} = f(x_k, u_k) + w_k$ and $z_k = g(x_k) + v_k$ respectively. In the case of EKF, the state transition matrix A in the Kalman filter is replaced by the linearization of f around the previous estimate $\hat{x}_{k-1}$, and the measurement matrix is replaced by linearizing the measurement model g around the current measurement z_k. Mathematically, we have

$$A_k = \frac{\partial f}{\partial x}|_{\hat{x}_{k-1}, u_k}, \tag{2.13}$$

$$H_k = \frac{\partial g}{\partial x}|_{\bar{x}_k}, \tag{2.14}$$

In addition, the innovation in the EKF is computed as

$$z_k - g(\bar{x}_k) \tag{2.15}$$

2.5 Two-Way Time Transfer

Time transfer is a key technique for generating, distributing, and synchronizing clocks across different sites [26, 27]. The purpose of time transfer is to determine the difference in clock readings, after which adjustments can be made to synchronize the clocks. The famous examples include the Network Time Protocol [28], the creation of International Atomic Time

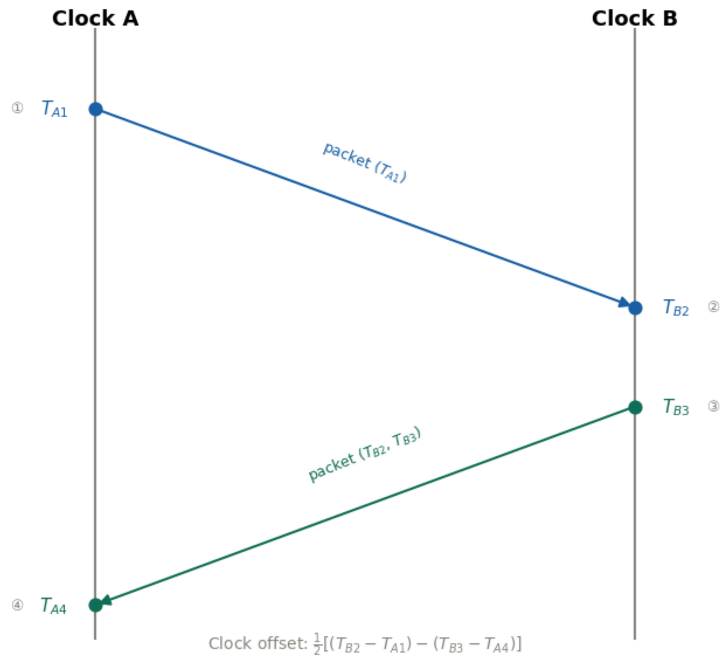

Figure 2.2: Visualization of two-way time transfer

(TAI) [29], and GNSS time transfer [30]. There are different schemes of time transferring, and two-way time transfer (TWTT) is widely used since it's able to compensate for the transmission delay. The overall flow is shown in Figure 2.2.

The TWTT is computed using the timestamps of signal transmission and reception. Considering two clocks A and B with readings $T_A(t)$ and $T_B(t)$, also treat clock B as the reference. The TWTT procedure is summarized as follows: 1. At T_{A1}, clock A sends a packet to B with timestamp T_{A1}. 2. Clock B recieved the packet and timestamp with it with T_{B2}. 3. Clock B sends the packet back to A at T_{B3}. 4. Clock A recieved the siganl and timestamp it T_{A4}. If the transmission delay is known or can be estimated, the clock difference between A and B is computed as

$$\Delta_{AB} = \frac{1}{2}(T_{B2} - (T_{A1} + T_{AB})) - \frac{1}{2}(T_{A4} - (T_{B3} + T_{BA})), \tag{2.16}$$

where T_{AB} and T_{BA} are the transimission delay. If the communication delay is symmetric, the above equation can be simplified to

$$\Delta_{AB} = \frac{(T_{B2} - T_{A1}) + (T_{B3} - T_{A4})}{2}. \tag{2.17}$$

2.6 Graph theory and consensus protocol

Graph theory is an effective framework for modeling the information exchange and control for a network of agents [31, 32, 33, 34]. Figure 2.3 shows an example of undirected graphs. An undirected graph is defined as $\mathcal{G} = \{\mathcal{V}, \mathcal{E}\}$ where $\mathcal{V}$ is the set of nodes and $\mathcal{E}$ is the set of edges connecting the nodes. The pair $(i, j) \in \mathcal{E}$ only exists if there exists an edge between node i and node j. It is common to represent and analyze the graph in matrix form; the most frequently used matrices are the adjacency matrix, degree matrix, and Laplacian matrix. An adjacency matrix A defined by

$$A_{ij} = \begin{cases} 1, & \text{if } \{i, j\} \in \mathcal{E}, \\ 0, & \text{otherwise.} \end{cases} \tag{2.18}$$

describes the connection relation between nodes. The degree matrix D is defined as

$$D_{ij} = \begin{cases} \deg(v_i), & \text{if } i = j, \\ 0, & \text{otherwise.} \end{cases} \tag{2.19}$$

where $\deg(v_i)$ represent the number of edges connected to node i. Finally, the Laplacian matrix L is defined as

$$L = D - A. \tag{2.20}$$

The other two useful variants of the Laplacian matrix in the literature are the normalized Laplacian and the left normalized (random walk) Laplacian matrix, which are defined as

$$L_{\text{normalized}} = D^{-\frac{1}{2}} L D^{-\frac{1}{2}} = I - D^{-\frac{1}{2}} A D^{-\frac{1}{2}} \tag{2.21}$$

$$L_{\text{normalized}} = I - D^{-1} A, \tag{2.22}$$

respectively. The consensus protocol is the foundation of distributed control; it aims to drive a group of agents with certain dynamics to reach an agreement state [35, 32, 36]. For a group of N agents communicates through a set of links described by a graph $\mathcal{G}$, and each agent follows the simple dynamic

$$\dot{x}_i = u, \quad i = 1, \dots, N \tag{2.23}$$

The consensus algorithm in continuous time is implemented as

$$\dot{x}_i = \sum_{j \in \mathcal{N}_i} (x_j - x_i), \tag{2.24}$$

where $\mathcal{N}_i$ correspond to the neighbors that connects to node i. If stacking all the agents' states into a column vector $x = [x_1, \dots, x_N]^T$, the consensus algorithm can be represented as

$$\dot{x} = -Lx \tag{2.25}$$

Correspondingly, the discrete-time consensus protocol is implemented as

$$x_i[k+1] = x_i[k] + \alpha \sum_{j \in \mathcal{N}_i} (x_j[k] - x_i[k]) \tag{2.26}$$

or

$$x(k+1) = (I - \alpha L)x(k), \tag{2.27}$$

where α satisfying $0 < \alpha \leq \frac{1}{\Delta}$ and Δ is the maximum degree of the graph. A **walk** in a graph is defined by a finite sequence $w = v_0 e_0 \dots e_N v_N$ that alternates between the nodes and edges. A **path** is a walk that with the nodes $v_1, \dots, v_N$ distinct and the edges $e_1, \dots, e_N$ distinct. A graph is said to be connected if there exists a path between each pair of nodes.

The convergence and convergence rate depend on the graph's connectivity, which can be determined by the spectral properties of the Laplacian matrix. The two theorems introduced below reveal some connections. Some additional discussion over the proof convergence and graph structure is shown in Appendix B.

Theorem 1. *Let $\lambda_1, \dots, \lambda_N$ be the eigenvalues of the Laplacian matrix L in ascending order. For a connected graph, it must satisfy $\lambda_1 = 0$ and $\lambda_i > 0$ for $i \geq 2$.*

Theorem 2. *For a connected graph, the consensus protocol 2.23 and 2.26 will converge to agreement with a convergence rate bounded by $\lambda_2(L)$.*

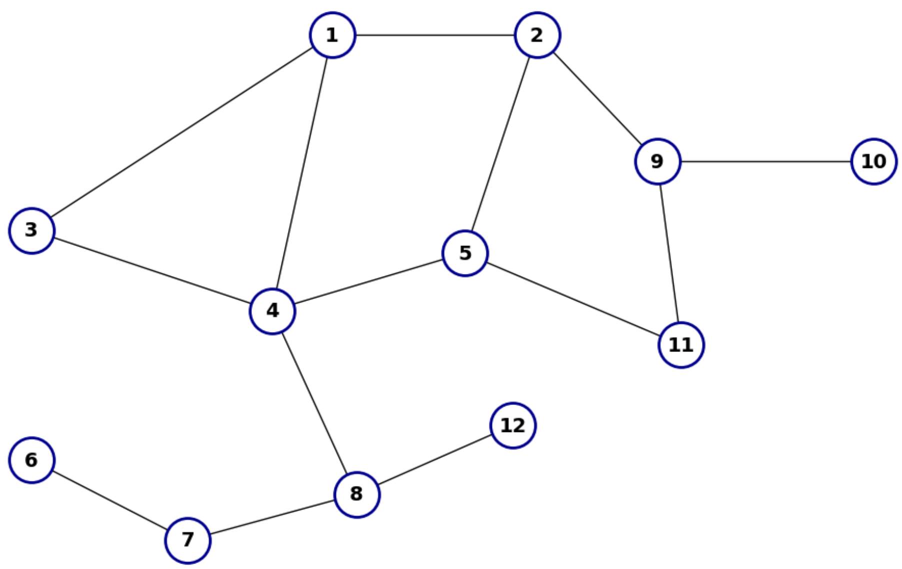

Figure 2.3: Undirected graph with 12 vertices and 14 edges

Chapter 3

MIXED CLOCK ENSEMBLE

This chapter introduces a mixed clock ensemble. The purpose of a mixed clock ensemble is to create a time scale with long-term stability given a group of clocks. The GPS time scale is generated by assembling all the clocks onboard the satellites and on the ground station [37, 38]. There are several advantages of using the mixed clock ensemble. First, it provides better stability performance than single clocks. Second, the computed ensemble clock is robust to a single clock's failure in the group. Lastly, the future timing system may consist of different types of clocks or oscillators for costs and specific mission requirements considerations.

The clock ensemble is achieved through computing the implicit ensemble means (IEM) of a group of clocks, which, depending on the estimation of the states of all the clocks from a Kalman filter, then compute their weighted sum [39, 40, 41]. Due to the unobservability of the true state of the clock, the IEM computed cannot be achieved directly. Therefore, the second Kalman filter will be used to estimate the difference between a controlled clock's state and the IEM, then by employing controls to the controlled clock to track the virtual reference.

This chapter describes the two Kalman filters for IEM computation and realization, respectively, as well as the control method to steer the oven-controlled quartz oscillator (OCXO) to track the IEM. The overall procedure is shown in Figure 3.1 [1]. Then, numerical simulations in different setup and demonstrate the effectiveness of the ensemble algorithm and its realization through control. Finally, we discussed the shortage and its possible application for future PNT satellite systems. Figure 1.2 showed the two clocks that was used in this work.

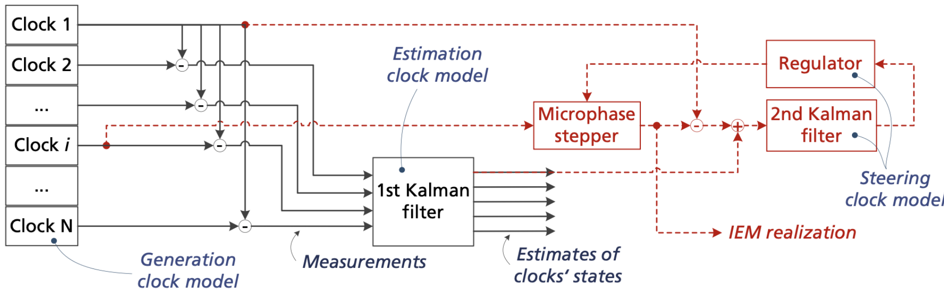

Figure 3.1: Clock ensemble and realization[1]

3.1 Implicit Ensemble Mean

Given a group of N clocks, the implicit ensemble mean(IEM) is a weighted average of the difference between the true clock phase and estimated clock phase, given by

$$\mathbf{IEM}(t_k) = \sum_{i=1}^{N} a_i(t_k)(x_i(t_k) - \hat{x}_i(t_k)), \tag{3.1}$$

where $a_i(t_k)$ and $\hat{x}_i(t_k)$ are from the Kalman filter that estimates the states for all the clocks in the group.

The state vector for the Kalman filter is

$$X = \begin{bmatrix} x_1 & y_1 & x_2 & y_2 & \dots & x_N & y_N \end{bmatrix}^T. \tag{3.2}$$

The state transition matrix is defined as

$$\Phi = \mathrm{diag}(A, A, ..., A) \tag{3.3}$$

where each A has the form of

$$A = \begin{bmatrix} 1 & \tau \\ 0 & 1 \end{bmatrix} \tag{3.4}$$

introduced in the clock model section.

The process noise covariance matrix is constructed similarly:

$$\mathbf{Q} = \mathrm{diag}(Q_1, Q_2, ..., Q_N), \tag{3.5}$$

where each Q_i is constructed in the way described in 2

As mentioned in the clock model section, the phase and frequency offset of the clock are not observable. For a group of clocks, the only measurable item is the phase difference reading between two clocks, which is also the phase difference between two clocks. For example, consider two clocks with clock readings $H_1(t)$ and $H_2(t)$, through comparing the clock readings, we obtain the measurement z_{12} as

$$z_{12} = H_1(t) - H_2(t) = (t + x_1(t)) - (t + x_2(t)) = x_1(t) - x_2(t). \tag{3.6}$$

In a group of N clocks, one of the clocks will be chosen as a reference and compared with the others in the ensemble. The choice of the reference clock can be arbitrary as it does not affect the results of the IEM. In this work, we consider the first clock in the ensemble as the reference clock, and the measurement matrix for the Kalman filter is therefore

$$H = \begin{bmatrix} -1 & 0 & 1 & 0 & \dots & & \\ -1 & 0 & 0 & 0 & 1 & 0 & \dots \\ \vdots & & & & & & \\ -1 & 0 & 0 & 0 & \dots & 1 & 0 \end{bmatrix}, \tag{3.7}$$

and the measurement vector is

$$z = \begin{bmatrix} z_{12} & z_{13} & \dots & z_{1N} \end{bmatrix}^T. \tag{3.8}$$

Since each of the measurements are independent, the measurement noise covariance can be constructed as

$$R = \begin{bmatrix} v_1, 0, \dots, 0 \\ 0, v_2, \dots, 0 \\ \vdots \\ 0, \dots, v_{N-1} \end{bmatrix} \tag{3.9}$$

with each of v drawn from a distribution depends on the setting.

Thus far, we've defined all the necessary elements for the Kalman filter to estimate the states of a group of N clocks, they are: the state vector X, state transition matrix Φ, measurement model H, measurement vector z, process noise covariance $\mathbf{Q}$, and measurement noise covariance R. At each time step, with the state estimation done, the weighted vector $a(t_k)$ is defined as

$$a(t_k) = \frac{P_{\phi\phi}^{-1}\mathbf{1}}{\mathbf{1}^T P_{\phi\phi}^{-1}\mathbf{1}}. \tag{3.10}$$

The matrix $P_{\phi\phi}$ is constructed using the components related to the phase offset of each clock in the estimated covariance matrix $\hat{P}$.

It is worth noting that due to the state observability, the estimation covariance grows over time. Therefore, it is necessary to perform covariance reduction here. Different covariance reduction techniques have been introduced in the literature [42]. The work uses

$$\begin{aligned} \tilde{P} &= S\hat{P}S^T, \\ \hat{P} &= \frac{1}{2}(\tilde{P} + \tilde{P}^T), \end{aligned} \tag{3.11}$$

The matrix S is an identity matrix with size $2N \times 2N$ that deletes the phase components in the estimation covariance matrix:

$$S = \begin{bmatrix} 0 & 0 & 0 & \cdots & 0 \\ 0 & 1 & 0 & \cdots & 0 \\ 0 & 0 & 0 & \cdots & 0 \\ \vdots & \vdots & \vdots & \ddots & \vdots \\ 0 & 0 & 0 & \cdots & 1 \end{bmatrix} \tag{3.12}$$

3.2 *Steering OCXO for IEM Realization*

From the definition of the **IEM**, we can see it relies on the true phase offset of the clock, which is unknown, so the **IEM** can not be achieved directly. Therefore, the realization is done by steering another clock to track the **IEM**. The steered clock is usually an oven-controlled crystal oscillator (OCXO) clock. The dynamical model for the OCXO clock is identical to the ones that were introduced above, but with an extra control term

$$\begin{bmatrix} x(t_{k+1}) \\ y(t_{k+1}) \end{bmatrix} = \begin{bmatrix} 1 & \tau \\ 0 & 1 \end{bmatrix} \begin{bmatrix} x(t_k) \\ y(t_k) \end{bmatrix} + \begin{bmatrix} \tau \\ 1 \end{bmatrix} u + w. \tag{3.13}$$

The control term u is a scalar value that can be computed using various methods, such as pole placement and linear quadratic Gaussian (LQG). The LQG method is utilized in this work and will be discussed later on.

Denote the state for the controlled clock as $[x_c(t_k), y_c(t_k)]^T$. Also denote the state of the reference clock from the ensemble and its estimation as $[x_{ref}(t_k), y_{ref}(t_k)]^T$, and $[\hat{x}_{ref}(t_k), \hat{y}_{ref}(t_k)]^T$ respectively. As the phase offset of the controlled clock is also unknown, steering this clock to track the **IEM** requires the difference or estimate of the difference between $x_c(t_k)$ and $\mathbf{IEM}(t_k)$. Define

$$\xi(t_k) = \Big[\xi_1(t_k), \xi_1(t_k)\Big]^T = \Big[x_c(t_k) - \mathbf{IEM}(t_k), y_c(t_k) - \tfrac{d\mathbf{IEM}(t_k)}{dt}\Big]^T. \tag{3.14}$$

The goal here is to drive the state ξ_1 to 0. Since ξ_1 is unknown, another Kalman filter is needed to estimate this state. The dynamical model is identical to the two-state clock model:

$$\xi(t_{k+1}) = A\xi(t_{k+1}) + Bu(t_k) + w, \tag{3.15}$$

with $w \sim \mathcal{N}(0, Q)$.

By the definition of the implicit ensemble mean, we can obtain the following relationship

$$\hat{x}_{ref}(t_k) = x_{ref}(t_k) - \mathbf{IEM}(t_k) + e(t_k), \tag{3.16}$$

where $e(t_k)$ is the error between the true offset and the IEM captured by the estimate error covariance. In this case, $e(t_k)$ is modeled as a random variable drawn from $N(0, \hat{P}[0,0])$. By comparing the controlled clock and the reference clock, we obtain

$$z_{c,ref} = x_c - x_{ref} + v(t_k), \tag{3.17}$$

with the $v(t_k)$ stands for the measurement noise. Adding up Eq 3.16 and Eq 3.17, get

$$\hat{x}_{ref}(t_k) + z_{c,ref} = [x_c(t_k) - \mathbf{IEM}(t_k)] + e(t_k) + v(t_k) = \xi_1(t_k) + e(t_k) + v(t_k) \tag{3.18}$$

This serves as the measurement model for the Kalman filter, where the measurement output is

$$\tilde{z} = \hat{x}_{ref}(t_k) + z_{c,ref}, \tag{3.19}$$

and the measurement matrix is

$$\tilde{H} = \begin{bmatrix} 1 & 0 \end{bmatrix}. \tag{3.20}$$

The measurement noise is computed as

$$\tilde{v}(t_k) = e(t_k) + v(t_k), \quad e(t_k) \sim \mathcal{N}\left(0, \hat{P}_{[0,0]}\right), \quad v(t_k) \sim \mathcal{N}(0, R). \tag{3.21}$$

Thus, all the parameters for the second Kalman filter to estimate ξ_1 are defined: the dynamic model 3.15, measurement model $\tilde{H}$, measured value $\tilde{z}$, the process noise covariance Q, and the measurement noise covariance $\tilde{R} = \hat{P}_{[0,0]} + R$. It is worth noting that the same covariance reduction technique as shown in Eq 3.11 is needed for this second Kalman filter with S matrix simply

$$S = \begin{bmatrix} 0 & 0 \\ 0 & 1 \end{bmatrix}. \tag{3.22}$$

With the estimated state $\hat{\xi}$ from the second Kalman filter, the linear quadratic Gaussian (LQG) control is utilized in this work to steer the OCXO clock. The LQG regulator $\hat{K}$ is first computed through solving the steady-state Ricatti equation

$$\hat{K} = A^T \hat{K} A + W_Q - A^T \hat{K} B (B^T \hat{K} B + W_R)^{-1} B^T \hat{K} A, \tag{3.23}$$

where W_Q and W_R are the penalties for states and control. The control gain is then

$$\hat{G} = (B^T \hat{K} B + W_R)^{-1} B^T \hat{K} A, \tag{3.24}$$

and the control value is

$$u = -\hat{G}\hat{\xi}(t_k). \tag{3.25}$$

The estimation and control gain computation for the controlled clock is performed with a certain interval.

3.3 Simulation

The simulation aims to validate the ensemble's stability and the effectiveness of the control law. The simulations use two types of clocks: Rubidium (Rb) atomic clocks and oven control crystal oscillators (OCXO). The Rubidium atomic clock is considered to be highly accurate and long-term stable; it is also used on GPS satellites. While the OCXO has higher short-term stability and the capability of controlling its frequency by varying the temperature.

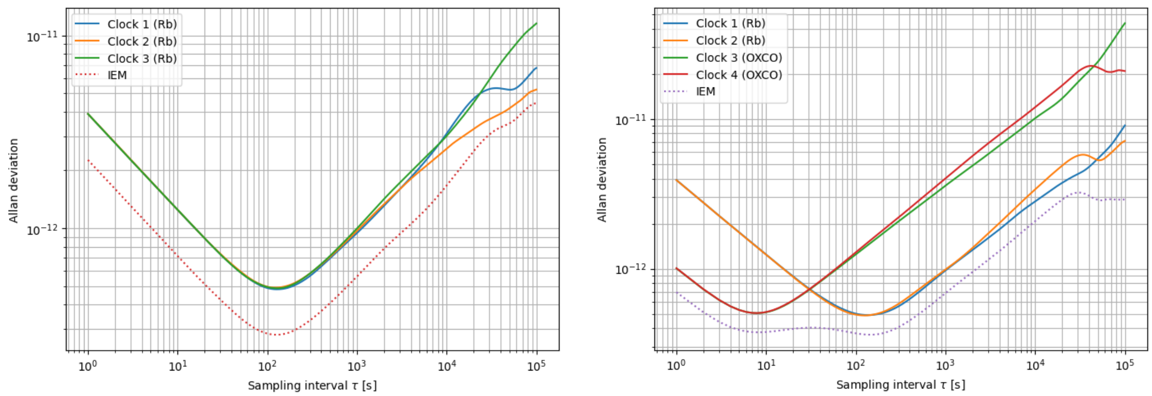

(a) Clock ensemble of 3 Rb atomic clocks (b) Ensemble of 2 Rb atomic and 2 OCXO clocks

Figure 3.2: Clock ensemble with different settings

The parameters are $\sigma_1^2 = 1.53 * 10^{-23}$, $\sigma_2^2 = 2.8 * 10^{-27}$, and $\sigma_1^2 = 10^{-24}$, $\sigma_2^2 = 5 * 10^{-26}$ for Rb and OCXO respectively. The phase offset of each clock is saved at each simulation time step for post-processing. Then the overlapping Allan variance (OADEV) for the time series of the phase offset data is computed and plotted on a log-log scale as the sampling interval varies. The discretization step $\tau = 1$s. The simulations were run for 72 hours.

Two cases for the clock ensemble are simulated. Case 1: an ensemble of 3 rubidium atomic clocks is simulated. Case 2: an ensemble of 4 clocks, consisting of 2 rubidium clocks and 2 OCXO clocks are computed and simulated, with one of the OCXO clock were chosen to be the reference. Next, the effectiveness of the clock control is validated by applying the LQG control to an OCXO clock outside the ensemble to track the IEM for both cases above. The LQG penalties is set to $W_Q = \begin{bmatrix} 0.35 & 0 \\ 0 & 0.07 \end{bmatrix}$ and $W_R = 1.9$. The steering is applied every 10 seconds. The results for the first and second ensemble is shown in Figure 3.2a and Figure 3.2b, respectively. The steering for realizing the IEM for both cases is shown in Figure 3.3a and 3.3b, respectively.

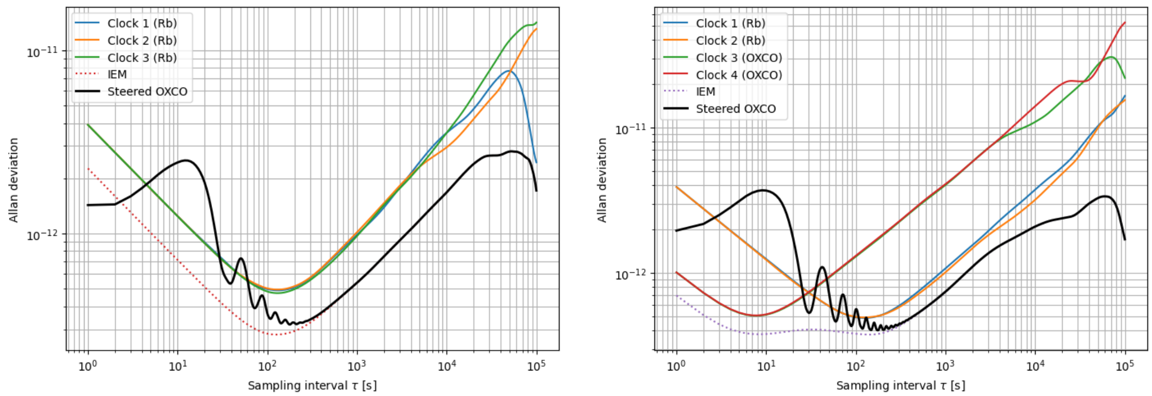

(a) Realization of clock ensemble of 3 Rb atomic clocks

(b) Realization of an ensemble of 2 Rb atomic and 2 OCXO clocks

Figure 3.3: Clock ensemble realization with different settings

3.4 Discussion

As the simulation demonstrated, the clock ensemble outperformed any single clock in the group. In a heterogeneous setting, the clock ensemble can combine the short-term and long-term stability of different clock types. The control method tracks the **IEM** and achieves long-term stability. To achieve stable clocks for the future satellite timing system, different architectures can be considered. For the PNT satellite systems that have a higher budget to equip multiple stability clocks, the clock ensemble can be conducted in the satellite independently to generate a time scale with higher stability. For the mega satellite constellation, the clocks on board could be cheap and unstable. In such a scenario, the inter-satellite link can be utilized to compare clocks between satellites to achieve higher stability. Further, one might consider using external sources,s such as GNSS clocks or ground station clocks, for ensembling, or bringing satellites equipped with higher stability clocks to achieve a mixed clock ensemble.

Chapter 4

ONBOARD CLOCK SYNCHRONIZATION VIA GNSS

Global Navigation Satellite System (GNSS) is a constellation of satellites that provides accurate positioning, navigation, and timing services. The most famous GNSS is the Global Positioning System (GPS) developed by the U.S. in the last century [4]. Some additional GNSS constellations also developed later [43], such as GLONASS (Russia), Bei Dou (China) [44], and Galileo (Europe). The GNSS satellites are equipped with multiple high-precision and stable clocks. These satellites usually operate in medium earth orbit (MEO), and the GNSS time is synchronized with the universal coordinated time (UTC).

There are considerable advantages to synchronizing the PNT satellite systems with the current GNSS systems. For LEO PNT constellations, the LEO satellites that are synced to the GNSS can serve as a relay for the GNSS time, while the LEO constellations are closer to the users, so the navigation signal can have lower propagation loss. Further, the LEO constellation usually has more satellites so that it can provide better coverage for PNT service. For the PNT satellite systems designed for extraterrestrial planet exploration, such as Lunar PNT and Mars PNT, synchronizing with the current GNSS systems enables better mission control, monitoring, and tracking for the ground control segment.

This chapter discusses how to use the pseudorange measurement from the GNSS satellites to synchronize the onboard clock of a satellite. Two methods for estimating receiver position and clock bias using the GNSS pseudorange measurements—nonlinear least squares and the extended Kalman filter (EKF)—are presented. Then, the numerical simulation of these two methods is demonstrated. Finally, we discussed the comparison of these two methods and the possible extensions for synchronizing the PNT satellite clock to the GNSS clocks.

4.1 Global Navigation Satellite System

The Global Positioning System (GPS) is constructed by a constellation of satellites in medium Earth orbit. The most common measurement provided by the GPS is the pseudorange measurement [45]. The pseudorange measurement at a time instant t is modeled as

$$\rho^{(k)} = r^k(t, t-\tau) + c[\delta t_u(t) - \delta t^{(k)}(t-\tau)] + I^{(k)}(t) + T^{(k)}(t) + \epsilon^{(k)}(t) \tag{4.1}$$

where $r^{(k)}(t, t-\tau)$ is the actual distance between the k-th GPS satellite and the receiver at the transmission time τ and reception time t; $\delta t_u(t)$ and $\delta t^{(k)}(t-\tau)$ are the clock bias of the GPS receiver and the GPS satellite clock; c is the speed of light; $I^{(k)}(t)$ and $T^{(k)}(t)$ are the ionospheric and tropospheric propagation error, and $\epsilon^{(k)}(t)$ accounts for other errors. For GPS receivers, the navigation message it receives contains: the GPS satellite clock bias $\delta t^{(k)}(t-\tau)$; the different types of propagation error. Therefore, accounting for this information leads to a simplified version of the pseudorange measurement

$$\rho^k = \|r^k - r\| + c\delta t_u + \epsilon \tag{4.2}$$

ϵ includes all the possible propagation errors. Notice that here $r^{(k)} = r^{(k)}(t-\tau)$ stands for the k-th satellite's position and signal transmission time $t-\tau$ and $r = r(t)$ stands for the postion of the reciver's position at measurement time t.

Depending on the position of the observer, the availability of a GNSS satellite is also constrained by the elevation angle of the GNSS satellite relative to the observer. This quantity is obtained by computing the zenith angle. Figure 4.1 showed a visualization of the zenith angle ξ. Denote the normalized position vector of the observer as $\mathbf{u} = \frac{r}{\|r\|}$, and the relative postion vector $\rho_i = \frac{r_i - r}{\|r_i - r\|}$. The zenith angle is defined as

$$\cos\xi_i = \rho_i^T \mathbf{u} \tag{4.3}$$

, and the elevation angle is defined as

$$E_i = 90^\circ - \xi_i \tag{4.4}$$

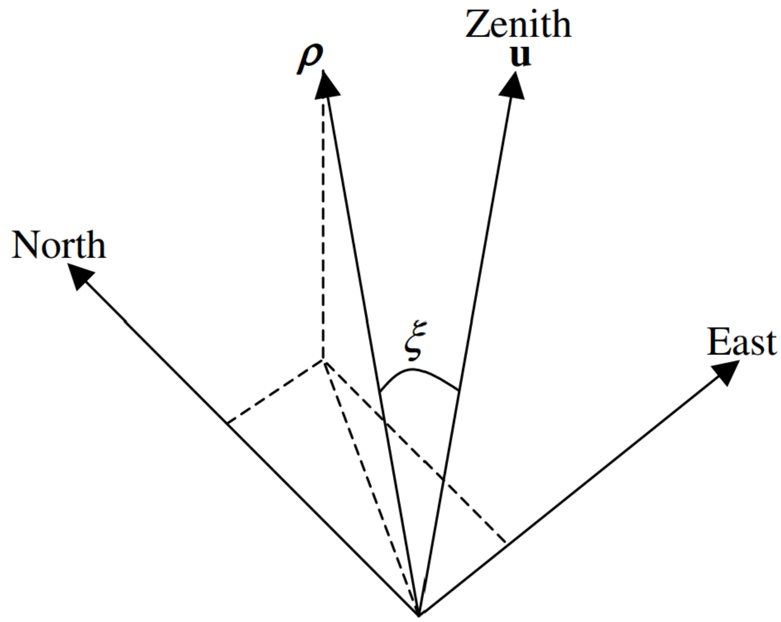

Figure 4.1: Visualization of the zenith angle

4.2 Nonlinear Least Square

The measurement model 4.2 is nonlinear due to the norm term. Using this measurement model, 4 elements of a satellite with a GPS receiver can be estimated: $[x, y, z, b]$ where the first three states describe the satellite's position and b is the clock offset multiplied by the speed of light $b = c\delta t_u$. Since there are 4 unknowns, at least 4 measurements are required to solve for the unknowns uniquely. To solve this estimation problem, the nonlinear least squares method can be utilized.

The Newton-Raphson method is an iterative method to solve the nonlinear least squares problem with initial guess $[x_0, y_0, z_0, b_0]$. Let $r_0 = [x_0, y_0, z_0]^T$. Define ρ_0^k as

$$\rho_0^k = \|r^k - r_0\| + b_0, \tag{4.5}$$

which is the approximate pseudorange based on the initial guess and the k-th satellite's position. Denote the true position and bias as r and b respectively. The following relationship $r = r_0 + \delta r$ and $b = b_0 + \delta b$ holds, where δr and δb are the unknown estimate error based on the current guess or estimate. By subtracting the measured pseudorange ρ_c^k and the approximated pseudorange, we obtain the following relationship

$$\begin{aligned}
\delta\rho^k &= \rho_c^k - \rho_0^k && (4.6)\\
&= \|r^k - (r_0 + \delta r)\| - \|r^k - r_0\| + (b - b_0) + \epsilon && (4.7)\\
&= \|r^k - r_0 - \delta r\| - \|r^k - r_0\| + \delta b + \epsilon && (4.8)
\end{aligned}$$

For the first term $\|r^k - r_0 - \delta r\|$, apply the first order approximation around δr

$$\begin{aligned}
&\|r^k - r_0 - \delta r\| && (4.9)\\
&\quad = \|(r^k - r_0) - \delta r\| && (4.10)\\
&\quad = \|r^k - r_0\| - \frac{r^k - r_0}{\|r^k - r_0\|} \cdot \delta r. && (4.11)
\end{aligned}$$

Plugging it back to equation 4.3, obtain

$$\delta\rho^k \approx -\frac{r^k - r_0}{\|r^k - r_0\|} \cdot \delta r + \delta b + \epsilon, \tag{4.12}$$

which is linear in δr and δb. Define

$$\mathbf{1}^k = \frac{r^k - r_0}{\|r^k - r_0\|}. \tag{4.13}$$

Then given K psuedorange measurements, we can write the 4.12 in matrix form

$$\delta\rho = \begin{bmatrix} \delta\rho^1 \\ \delta\rho^2 \\ \vdots \\ \delta\rho^K \end{bmatrix} = \begin{bmatrix} -\mathbf{1}^1 & 1 \\ -\mathbf{1}^2 & 1 \\ \vdots & \\ -\mathbf{1}^K & 1 \end{bmatrix} \begin{bmatrix} \delta r \\ \delta b \end{bmatrix} + \epsilon_k \tag{4.14}$$

Define

$$G = \begin{bmatrix} -(\mathbf{1}^1)^T & 1 \\ -(\mathbf{1}^2)^T & 1 \\ \vdots & \\ -(\mathbf{1}^K)^T & 1 \end{bmatrix} \tag{4.15}$$

as the geometry matrix. When K is exactly 4, the unknown vector $[\delta r, \delta b]^T$ can be solved using matrix inversion, i.e.

$$\begin{bmatrix} \delta r \\ \delta b \end{bmatrix} = G^{-1}\delta\rho.$$

In general, $K \geq 4$, $[\delta r, \delta b]^T$ can be solved as a least square problem

$$\min \|G \begin{bmatrix} \delta r \\ \delta b \end{bmatrix} - \delta\rho\|^2, \tag{4.16}$$

Which has a closed-form solution

$$\begin{bmatrix} \delta\hat{r} \\ \delta\hat{b} \end{bmatrix} = (G^T G)^{-1} G^T \delta\rho. \tag{4.17}$$

After $[\delta\hat{r}, \delta\hat{b}]^T$ are solved, the estimation $\hat{r}$ and $\hat{b}$ are updated by $\hat{r} = r_0 + \delta\hat{r}$ and $\hat{b} = b_0 + \delta\hat{b}$. This procedure is then repeated iteratively when two consecutive estimations have a norm distance smaller than some predefined threshold ϵ. Here, the geometry matrix reveals an important relationship between the GPS satellite geometry and precision of the estimation; additional discussion is shown in Appendix A.

4.3 Extended Kalman Filter

For a LEO satellite in orbit, an extended Kalman Filter approach can be utilized. The state vector for the EKF is $x = [r, v, b, \dot{b}]$, where $r = [r_x, r_y, r_z]^T$ and $v = [v_x, v_y, v_z]^T$ are the position and velocity of the satellite respectively, b and $\dot{b}$ are the phase and frequency drift times the speed of light. In this work, we assume the position and velocity of the receiver LEO satellite satisfy the following approximated two-body dynamics [46, 47]:

$$\dot{r} = v \tag{4.18}$$

$$\dot{v} = -\frac{\mu}{\|r\|^3} r + w \tag{4.19}$$

where $\mu = GM$, and G is the gravitaional constant of the earth, M is the mass of the Earth. The dynamics for b and $\dot{b}$ follow the linear dynamics introduced in equation 2.3. The w corresponds to the noise and perturbation for the dynamics. To fit the dynamic into the discrete-time EKF framework, the continuous-time dynamics can be discretized in different ways, such as the Euler method or the Runge-Kutta method.

The measurement model $h(x)$ is given by 4.2. To construct the observation matrix for the EKF, the linearization procedure introduced in section 4.3 is utilized to linearize around the predicted state using the known GPS satellite positions. The measurement vector is the concatenation of the pseudorange measurements $z_k = [\rho_k^1, \rho_k^2, \ldots, \rho_k^N]$.

4.4 Simulations

In this section, both of the methods introduced above were simulated for a LEO satellite, assuming it has the capability of receiving GPS signals. Python is used to simulate the orbital propagation of the test satellites and the GPS satellite, GPS satellite visibility, and pseudorange measurement. The test satellite is STAR-LINK 1012 from the Starlink constellation.

The simulation is done in a discretized manner with a time step $\Delta t = 1s$ and runs for 3600 seconds. The procedure for simulating the application of the two methods is as follows. First, determine the initial position and velocity of the GPS satellites and the receiver satellites resolved in the Earth Centered Inertia (ECI) frame using the up-to-date TLE file from the Celestrack website [48]. The GPS satellite state vector $[r, v]^T$ is propagated forward using the high-fidelity SGP4 propagator from the Skyfield package [49]. The ground truth trajectory of the test satellite is propagated using 4.18 and 4.19. The GPS time is assumed to be equal to the true time and initialized to 0 at the start of the simulation, i.e., $t_{GPS} = t$ and evolves with $t_{GPS}(t_{k+1}) = t_{GPS}(t_k) + \Delta t$. The test satellite's clock reading t_{test}, clock bias ϕ, and frequency drift $\dot{\phi}$ are initialized to 0, and the clock propagates with the clock dynamics 2.3. The perturbation for 4.19 is assumed to be a Gaussian noise here. The process noise covariance for the position and velocity state r and v is

$$Q_{pos} = \mathbf{diag}(1e^{-8}, 1e^{-8}, 1e^{-8}, 1e^{-12}, 1e^{-12}, 1e^{-12})$$

and the noise covariance of the clock satisfying $Q_{clk} = \begin{bmatrix} s_{ph} + \frac{s_{fr}}{3} & \frac{s_{fr}}{2} \\ \frac{s_{fr}}{2} & s_{fr} \end{bmatrix}$ with $s_{ph} = 0.00007$

and $s_{fr} = 0.000001$. The error covariance matrix for the EKF is initialized to

$$P = \mathbf{diag}(1.0, 1.0, 1.0, 1e^{-4}, 1e^{-4}, 1e^{-4}, 1e^{-6}, 1e^{-8})$$

with position and velocity in units of km and km/s. Next, at each time step, given the positions of the GPS and test satellites, the elevation cutoff angle introduced in 4.4 is set to 15°. With the available GPS satellites, the pseudorange measurement is simulated using equation 4.2 with a measurement noise covariance of $R = 10^{-4}$. The linearization for the nonlinear dynamic is done using the automatic differentiation tool from the Python Jax library [50]. The termination condition ϵ for the nonlinear least squares is set to 1×10^{-6}. Finally, the estimation using the nonlinear least squares and EKF is performed at each time step.

Figures 4.2 and 4.3 illustrate the estimated position and clock-bias profiles obtained from both the Nonlinear Least Squares (NLS) method and the Extended Kalman Filter (EKF), while Figures 4.4 and 4.5 present the corresponding estimation error histories for position and clock bias, respectively.

Regarding position estimation accuracy, the NLS method yields a mean error of 0.8813 km with a variance of 0.2348 km^2. The EKF produces a mean position estimation error of 0.0723 km with a variance of 0.0029 km^2.

With respect to clock bias estimation, the NLS method achieves a mean error of 1.7158×10^{-6} s and a variance of 1.7272×10^{-12} s^2. The EKF exhibits a mean clock bias error of 7.7629×10^{-7} s and a variance of 5.33904×10^{-13} s^2.

4.5 Discussion

In this chapter, we discussed two methods for synchronizing satellite clocks with GNSS time and presented numerical simulations for both to verify their effectiveness and compare their performance. As can be observed from the simulation results, the Extended Kalman filter method demonstrates better estimation accuracy, smoothness, and consistency. The Extended Kalman filter has the ability to incorporate the dynamics for prediction.

Both of the methods discussed in this chapter only use the pseudorange measurement. In addition to pseudorange measurements, GNSS provides carrier phase and Doppler shift

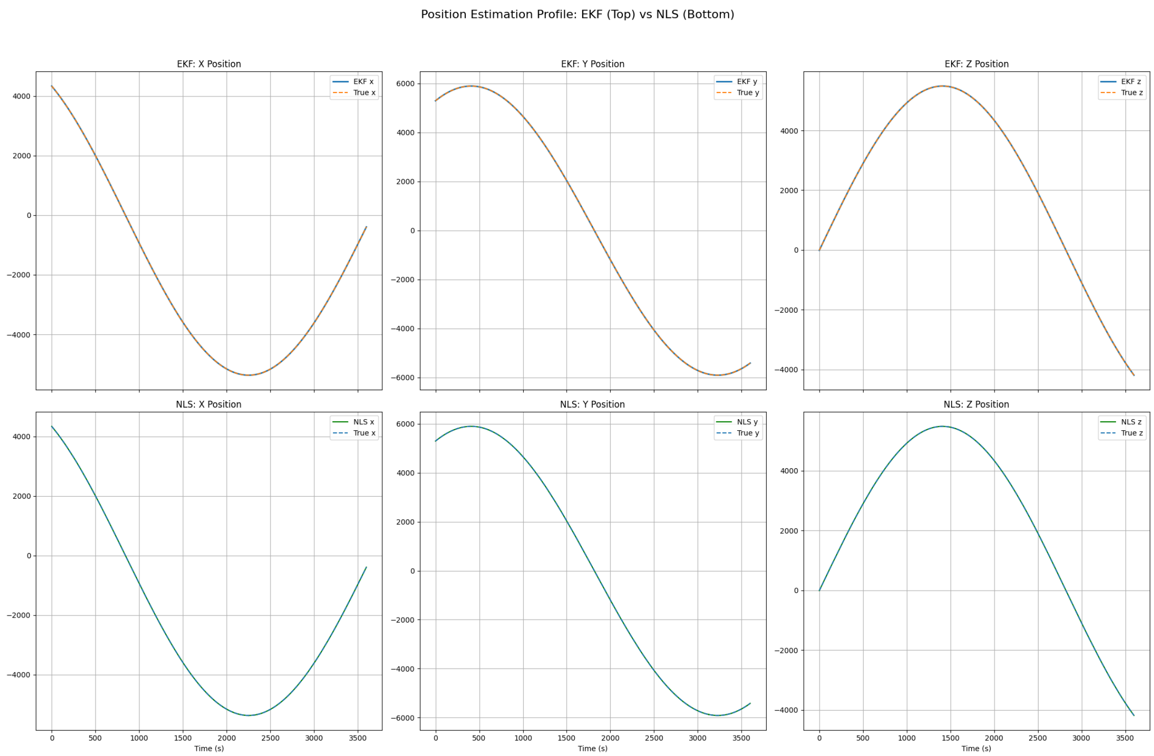

Figure 4.2: Position estimation profile

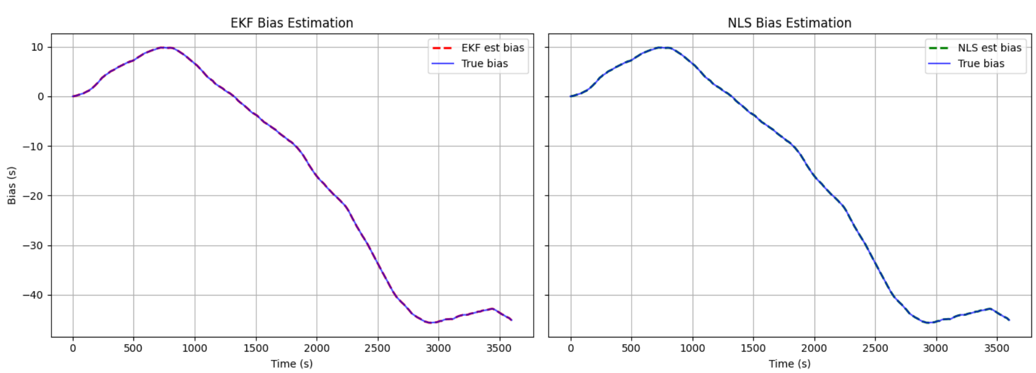

Figure 4.3: Bias estimation history for EKF and nonlinear least square

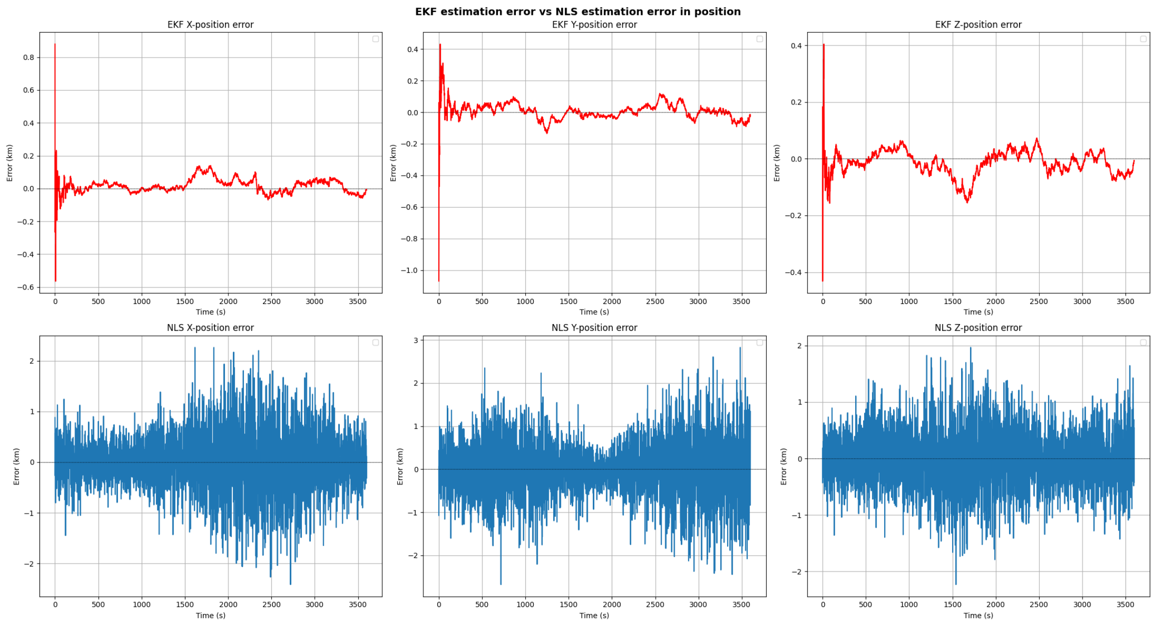

Figure 4.4: Position estimation error history

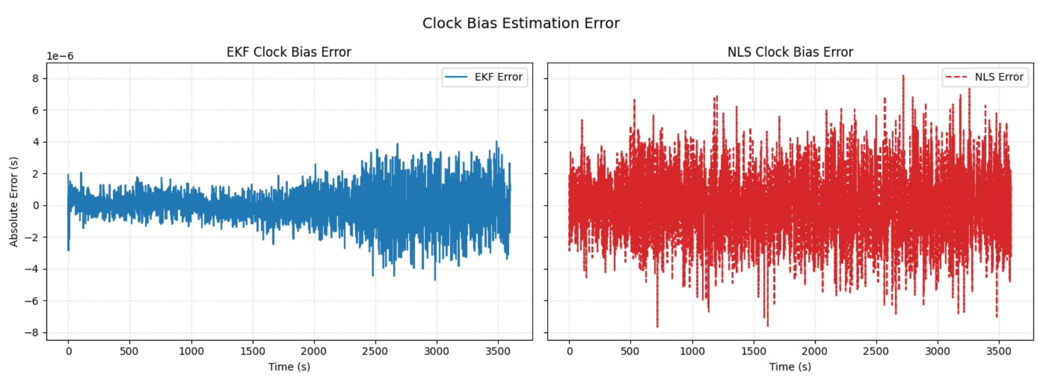

Figure 4.5: Bias estimation error history

measurements [51]. Combining these measurements enables the estimation of velocity and clock frequency drift, which can enhance the estimation of position and bias.

As synchronizing the PNT satellites to the current GNSS system provides considerable advantages, it also raises challenges for the PNT satellite constellation design, which requires further research. From the signal receiving perspective, the geometry design for the PNT satellite constellation so that the satellites can have access to the GNSS signals is important. This can be seen as an optimization that aimed to maximize the synchronization and estimation performance, while considering the constraints such as orbital mechanics, line-of-sight availability, and satellite positions. For the clock onboard the satellites, especially for the ones that are at lower prices, which are easy to drift due to temperature, radiation, and potentially the velocity of the satellite, the process covariance for such clocks is actually time varying. Therefore, for bias estimation, synchronization, and self-calibration of these cheap clocks, methods for capturing the variation in process noise must be developed.

Chapter 5

TIME SYNCHRONIZATION OVER SATELLITE CONSTELLATION VIA INTER-SATELLITE LINKS

This chapter presents the concepts of using an inter-satellite link to achieve clock synchronization over a satellite constellation. An inter-satellite link establishes communication between satellites, enabling two-way time transfers between them [52, 53]. For PNT satellite systems, the vital requirement for accurate positioning is that the clocks of the constellation are synchronized. In the case of the absence of an external clock reference, such as GNSS or ground segment, utilizing the Inter-satellite link can achieve synchronization within the constellation, which improves the robustness and reliability of the positioning service. On the other hand, if all or part of the PNT constellation is equipped with a GNSS receiver, the inter-satellite link can enhance the propagation of the GNSS time over the PNT satellite constellations, providing potential solutions to the time synchronization problem caused by part of the satellites being unable to receive GNSS signals. For example, for Lunar PNT, a satellite equipped with both an ISL and a GNSS receiver can be placed in a proper position designed to serve as a relay for the PNT satellite that is occulted by the moon.

In this chapter, we first present a proportional-integrating (PI) consensus algorithm [54] that can be used for tuning clocks dynamically for synchronization. We then performed a study on the relationship between the inter-satellite link and the synchronization performance. The chapter will finish with a discussion over the analysis of the simulated results and the future of using ISL for clock synchronization for PNT constellations.

5.1 Synchronization using PI Consensus Algorithm

The synchronization algorithm aims to align the clock's reading continuously. Consider the local clock reading models

$$T(t_k) = t_k + b(t_k) \tag{5.1}$$

, and its equivalent discrete-time clock reading dynamics

$$T(t_{k+1}) = T(t_k) + b(t_k) \tag{5.2}$$

where $T(t_k)$ represents the clock reading at time step k and $b(t_{k+1}) = \Delta t(y_i(t_k) + 1) + w_f$ describes the increment of local clock reading capturing the nominal increment by the step size, bias drift contributed by frequency drift, and a Gaussian process noise. This model is derived from 2.3 by

$$\begin{aligned} T_i(t_{k+1}) &= t_{k+1} + x_i(t_{k+1}) \\ &= t_k + \Delta t + (x_i(t_k) + \Delta t\, y_i(t_k) + w_f) \\ &= \big(t_k + x_i(t_k)\big) + [\Delta t(y_i(t_k) + 1)] + w_f \\ &= T_i(t_k) + b_i(t_k) + w_f \end{aligned} \tag{5.3}$$

.

Assuming each clock can be controlled by a local input $u_i(k)$ such that $T_i(k+1) = T_i(k) + b_i(k) + u_i(k)$. Defining N-dimentional vector $T(k)$, $b(k)$, and $u(k)$, where each components of the vector are $T_i(k)$, $b_i(k)$, and $u_i(k)$ respectively.The clock reading dynamic for the whole constellation is then

$$T(k+1) = T(k) + b(k) + u(k). \tag{5.4}$$

For this clock dynamics model, as both the drift and offset are time varying, the classic consensus dynamic 2.24 is unable to align both of the states. Therefore, a proportional-integrating (PI) consensus algorithm [54] can be used here. In this algorithm, an intermediate controller state w is introduced. The controller state for each agent is the following

$$w_i(k+1) = T_i(k) - \frac{\alpha}{|\mathcal{N}_i|} \sum_{j \in \mathcal{N}_i} K_{ij} T_j(k) \tag{5.5}$$

$$u_i(k) = w_i(k) - \frac{1}{|\mathcal{N}|_i} \sum_{j \in \mathcal{N}_i} K_{ij} T_j(k) \tag{5.6}$$

Where

$$\sum_{j \in \mathcal{N}} K_{ij} T_j(k) = \sum_{j \in \mathcal{N}} (T_i(k) - T_j(k)), \tag{5.7}$$

and α is a positive constant smaller than 1. The $|\mathcal{N}|$ denotes the cardinality of the neighbor set for agent i. As the classic consensus protocol, the PI consensus algorithm requires the state difference between agents. In this scenario, clock reading differences between satellites are required and can be determined using the two-way time transfer method introduced in Chapter 2.

The global system will become:

$$\begin{bmatrix} T(t_{k+1}) \\ w(t_{k+1}) \end{bmatrix} = \begin{bmatrix} I-K & I \\ -\alpha K & I \end{bmatrix} \begin{bmatrix} T(t_k) \\ w(t_k) \end{bmatrix} + \begin{bmatrix} b(t_k) \\ 0 \end{bmatrix} \tag{5.8}$$

with K being the left-normalized Laplacian matrix introduced in Chapter 2.

5.2 Proof of Convergence

The proof of the convergence of the PI consensus law follows a similar philosophy to the proof of the consensus protocol shown in Appendix B. This section goes over the proof of convergence of this consensus control law. Here, we assume that the graph is connected, and then the Laplacian matrix has the following eigenvalue properties

$$0 = \lambda_1 \leq \lambda_2 \leq \dots \lambda_N \leq 2. \tag{5.9}$$

In addition, for simplicity, here we assume the frequency drift $y_i(t_k)$ is a constant term and has the same for every agent, hence the $b_i(t_k) = \Delta t(y_i(t_k)+1) = b_i$ is a constant, and assuming no process noise.

Since the graph is assumed to be connected, the left-normalized Laplacian matrix can be performed eigendecomposition into

$$K = U\Sigma U^{-1}. \tag{5.10}$$

where $\Sigma = \mathbf{diag}(\lambda_1, \lambda_2, \dots, \lambda_N)$ is the diagonal matrix with entries being the eigenvalues of K and $U = [u_1|u_2|\dots|u_N]$ is the matrix consisting of right eigenvectors corresponding to the eigenvalues. The right eigenvector corresponding to $\lambda_1 = 0$ has the form of $u_1 = [1, \dots, 1]^T$. Denote $V = U^{-1}$ and $V = [v_1|v_2|\dots|v_N]^T$ where each row of V is the left eigenvector of K. For the left-normalized Laplacian of a connected graph, $v_1^T = \frac{1}{D_{total}}[d_1, \dots, d_N]$, where $D_{total} = \sum_{i=1}^N d_i$ are the sum of each agent's degree.

Defining new state vectors $\tilde{T} = U^{-1}T$, $\tilde{w} = U^{-1}w$, $\tilde{b} = U^{-1}b$, and $\tilde{y} = U^{-1}y$. The dynamic model 5.8 can be written as

$$\begin{bmatrix} \tilde{T}(t_{k+1}) \\ \tilde{w}(t_{k+1}) \end{bmatrix} = \begin{bmatrix} U^{-1}T(t_{k+1}) \\ U^{-1}w(t_{k+1}) \end{bmatrix} = U^{-1} \begin{bmatrix} I - U\Sigma U^{-1} & I \\ -\alpha U\Sigma U^{-1} & I \end{bmatrix} \begin{bmatrix} T(t_k) \\ w(t_k) \end{bmatrix} + U^{-1} \begin{bmatrix} b \\ 0 \end{bmatrix}. \tag{5.11}$$

and turned into

$$\begin{bmatrix} \tilde{T}(t_{k+1}) \\ \tilde{w}(t_{k+1}) \end{bmatrix} = \begin{bmatrix} I - \Sigma & I \\ -\alpha\Sigma & I \end{bmatrix} \begin{bmatrix} \tilde{T}(t_k) \\ \tilde{w}(t_k) \end{bmatrix} + \begin{bmatrix} \tilde{b} \\ 0 \end{bmatrix}. \tag{5.12}$$

Hence, the system can be decoupled into N individual systems

$$\begin{bmatrix} \tilde{T}_i(t_{k+1}) \\ \tilde{w}_i(t_{k+1}) \end{bmatrix} = \begin{bmatrix} 1 - \lambda_i & 1 \\ -\alpha\lambda_i & 1 \end{bmatrix} \begin{bmatrix} \tilde{T}(t_k) \\ \tilde{w}(t_k) \end{bmatrix} + \begin{bmatrix} \tilde{b}_i \\ 0 \end{bmatrix}. \tag{5.13}$$

Here we analyze the stability condition of the systems shown in 5.13. For the state transition matrix, we compute the characteristic polynomial:

$$p(z) = \det(zI - \begin{bmatrix} 1 - \lambda_i & 1 \\ -\alpha\lambda_i & 1 \end{bmatrix}) \tag{5.14}$$

$$= z^2 + (\lambda - 2)z + (\alpha\lambda + 1 - \lambda) \tag{5.15}$$

Since this system is in discrete time, applying the Jury stability criterion

$$p(1) > 0 \rightarrow \alpha\lambda > 0 \rightarrow \alpha > 0 \tag{5.16}$$

$$p(-1) > 0 \rightarrow 0 < \lambda < \frac{4}{2 - \alpha} \tag{5.17}$$

$$|\alpha\lambda + 1 - \lambda| < 1 \rightarrow \alpha < 1 \tag{5.18}$$

In summary, the stability condition is $0 < \alpha < 1$, and $0 < \lambda < \frac{4}{2-\alpha}$. In the case of using the left-normalized graph Laplacian, the eigenvalue satisfies $0 = \lambda_1 \leq \lambda_2 \leq \cdots \leq \lambda_N \leq 2$; therefore, with proper choice of α, the convergence is guaranteed.

With the parameters α properly set up, denote the steady-state for the transformed clock reading state and controller state of each subsystem as $\tilde{T}_i(\infty)$ and $\tilde{w}(\infty)$ for $i \neq 1$, we can solve the system

$$\begin{bmatrix} \tilde{T}_i(t_\infty) \\ \tilde{w}_i(t_\infty) \end{bmatrix} = \begin{bmatrix} 1 - \lambda_i & 1 \\ -\alpha\lambda_i & 1 \end{bmatrix} \begin{bmatrix} \tilde{T}_i(\infty) \\ \tilde{w}_i(\infty) \end{bmatrix} + \begin{bmatrix} \tilde{b}_i \\ 0 \end{bmatrix}. \tag{5.19}$$

Which can be turned into a linear equation

$$\begin{bmatrix} \lambda_i & -1 \\ \alpha\lambda_i & 0 \end{bmatrix} \begin{bmatrix} \tilde{T}_i(\infty) \\ \tilde{w}_i(\infty) \end{bmatrix} = \begin{bmatrix} \tilde{b}_i \\ 0 \end{bmatrix} \tag{5.20}$$

Solving this equation leads to $\tilde{T}_i(\infty) = 0$ and $\tilde{w}_i(\infty) = -\tilde{b}_i$ for $i \geq 2$. For $\lambda_1 = 0$, the equation 5.13 becomes

$$\begin{bmatrix} \tilde{T}_1(t_{k+1}) \\ \tilde{w}_1(t_{k+1}) \end{bmatrix} = \begin{bmatrix} 1 & 1 \\ 0 & 1 \end{bmatrix} \begin{bmatrix} \tilde{T}_1(t_k) \\ \tilde{w}_1(t_k) \end{bmatrix} + \begin{bmatrix} \tilde{b}_1 \\ 0 \end{bmatrix}, \tag{5.21}$$

which leads to $\tilde{T}_1(t_k+1) = \tilde{T}_1(t_k) + \tilde{b}_1$ and $\tilde{w}_1(t_{k+1}) = \tilde{w}(t_k) = 0$, and so $\tilde{T}_1(t_k) = k\tilde{b}_1 + \tilde{T}(0)$. By combining the derivation above, the transformed clock reading vector is

$$\tilde{T}(t_k) = [k\tilde{b}_1 + \tilde{T}_1(0), 0, \ldots, 0]^T. \tag{5.22}$$

as $t_k \to \infty$. By performing the inverse transform by multiplying U to both sides of equation 5.22, we obtain

$$\begin{aligned} T(t_k) = U\tilde{T}(t_k) &= U[k\tilde{b}_1 + \tilde{T}_1(0), 0, \ldots, 0]^T && (5.23) \\ &= u_1(k\tilde{b}_1 + \tilde{T}_1(0)) && (5.24) \\ &= u_1(kv_1^T b + v_1^T T(0)) && (5.25) \\ &= u_1 v_1^T (kb + T(0)) && (5.26) \\ &= \begin{bmatrix} v_1^T(kb + T(0)) \\ v_1^T(kb + T(0)) \\ \vdots \\ v_1^T(kb + T(0)) \end{bmatrix} && (5.27) \end{aligned}$$

, which indicates that all the individual clocks have the same value, thus consensus is achieved.

5.3 Information Exchange Networks

In this work, we assume the neighbor set for each satellite is determined by the distance between satellites and the inter-satellite link range r_a, which

$$N_i = \{j \in \mathcal{V} : \|p_j - p_i\| < r_a,\ j \neq i\}. \tag{5.28}$$

Under this assumption, the network formed by the satellite constellation is a time-varying network due to the motion of the satellites. Figures 5.1 and 5.2 showed the network construct by the satellites and ISLs under this assumption. Figure 5.1 and 5.2showed 500 and 900 satellites randomly drawn from the StarLink constellation, respectively, and ISL ranging is 1000km, 2000km, and 3000 km.

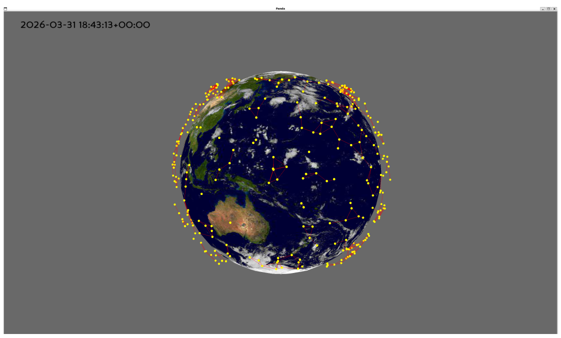

(a) Range = 1000 km

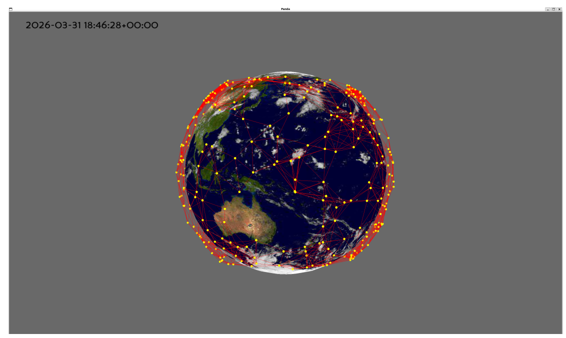

(b) Range = 2000 km

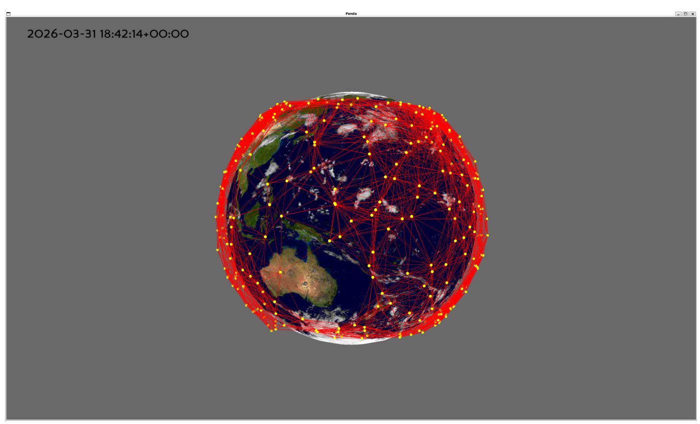

(c) Range = 3000 km

Figure 5.1: Satellite network with 500 satellites under different ISL ranges

5.4 Simulations and Results

For the numerical simulation, we implemented the PI consensus algorithm and tested it on a partial set of satellites from the Starlink constellation, where each of the satellites was

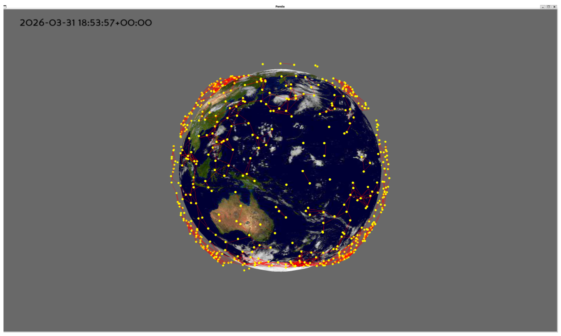

(a) Range = 1000 km

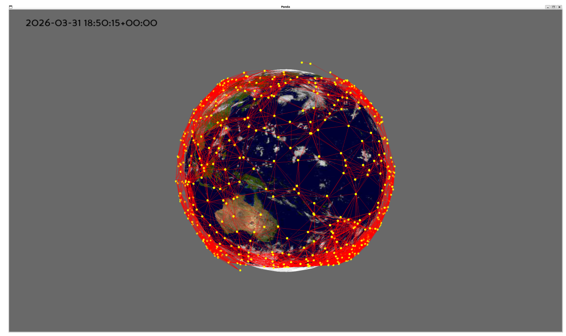

(b) Range = 2000 km

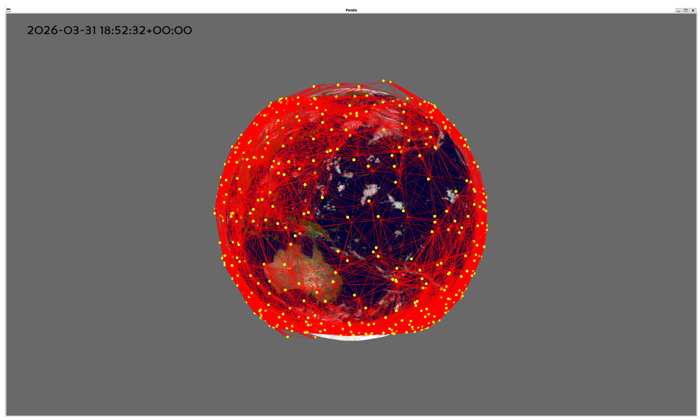

(c) Range = 3000 km

Figure 5.2: Satellite network with 900 satellites under different ISL ranges

running the consensus algorithm.

The simulation has been performed a Python environment, and the procedure is the following. First, we select a set of N satellites from the StarLink constellation randomly. Using the publicly available TLE data from the CelesTrak website [48] to determine their initial position. The positions of all the satellites are then propagated using the SGP4 propagator from the Skyfield package [49]. The clock readings of each satellite are initialized to values between 0 and 200 according to a uniform distribution. For simility, the frequency drift $y(t_k)$ is considered to be constant for the simulation, then the noisy increment term $b(t_k)$ is initialized to a value with mean $\Delta t = 1$ and variance 0.001. The process noise w_f

is a Gaussian noise with zero mean and variance 0.001. The simulation is run in time step $\Delta t = 1$ s, and the simulation horizon is 500 seconds. The coefficient α is set to 0.2.

Figure 5.3 shows the result of the simulation with 300 satellites and an inter-satellite link range of 1500 km, and 2100km, respectively. Figure 5.4 show the result of the simulation with 500 satellites and an inter-satellite link range of 1500 km, and 2100km, respectively.

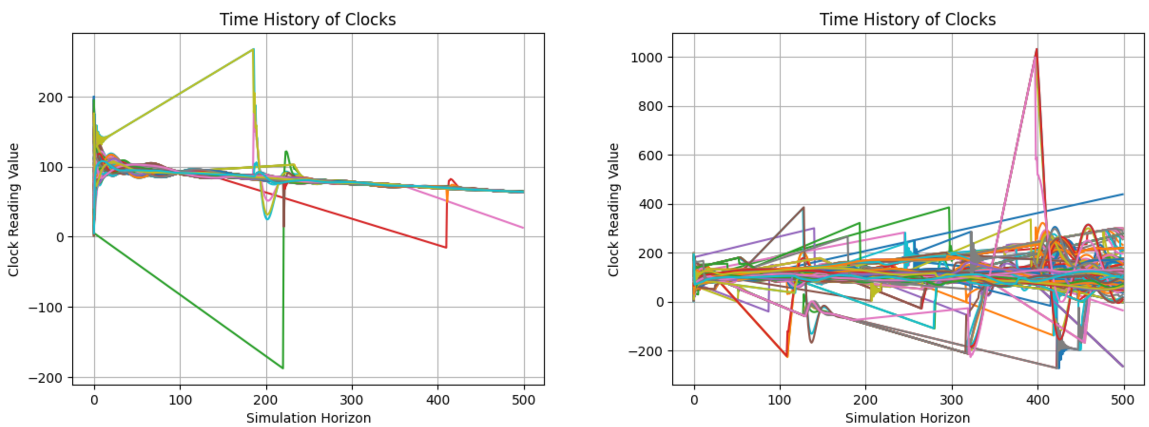

(a) ISL range 2100 km

(b) ISL range 1500 km

Figure 5.3: Consensus on 300 satellites for different ISL ranges

In addition to verifying the effectiveness of the consensus algorithm, we also examine the effect of the length of the inter-satellite link and the number of satellites on the consensus. Different combinations of the number of satellites and ISL range were tested. We tested N with value $[300, 500]$ and ISL range $[1500, 1700, 1900, 2100, 2300, 2500, 2700]$ kilometers. To evaluate consensus across different settings, the average variance of each satellite's clock reading relative to its average over the simulation horizon is computed. Figure 5.5 shows this metric in different ISL range distances and different numbers of satellites.

5.5 Discussion

In this chapter, a proportional-integrating consensus algorithm for clock synchronization is presented. The algorithm is then simulated over a subset of satellites from the StarLink

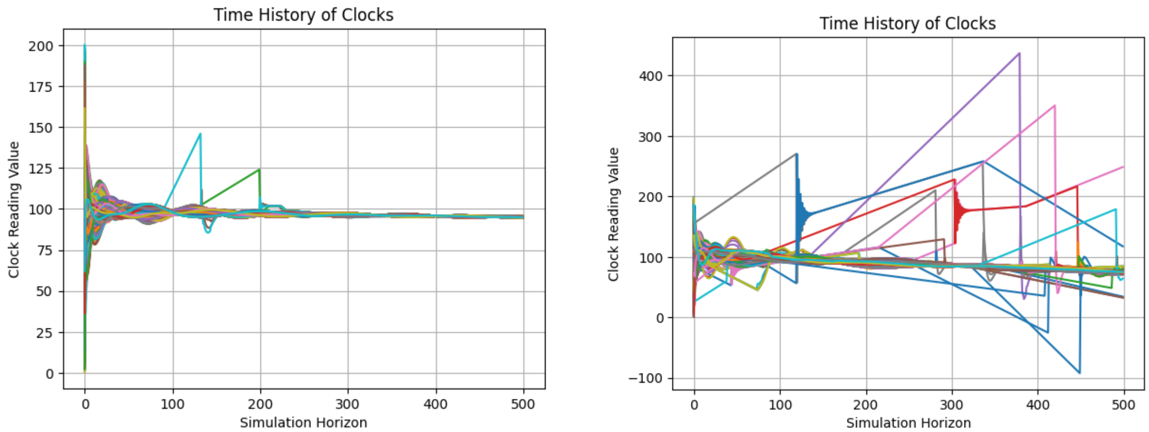

(a) ISL range 2100 km

(b) ISL range 1500 km

Figure 5.4: Consensus on 500 satellites for different ISL ranges

constellation, with a network formed based on the inter-satellite link ranges. The simulation is performed on 300 satellites and 500 satellites with an ISL range of 1500 km and 2500km. As shown in Figure 5.3 and Figure 5.4. The consensus algorithm is successfully driving all the clocks to a synchronized value with an ISL range of 2100 km. This indicates that the underlying graph of the network formed by the satellites is connected according to Theorem 2. It can be observed from Figure 5.3b and 5.4b that there are partial of the clocks failed to synchronize or diverge from the synchronization at some point of the simulation. This is due to the fact that when the ISL range is low, some of the satellites are isolated or form a cluster, which leads to divergence. It is also worth mentioning that the coefficient α is picked arbitrarily; this parameter can be picked in a more optimized way if the network structure is fixed, which may also be an interesting research direction in a dynamic network situation like the satellite constellations.

Due to the existence of the random process noise, the clocks are never synchronized to a steady state; instead, the consensus algorithm will bound the clock values within some boundary. The effect on the number of satellites and the ISL range distance on this bound is also investigated by computing the average variance of the clock readings over the simulation

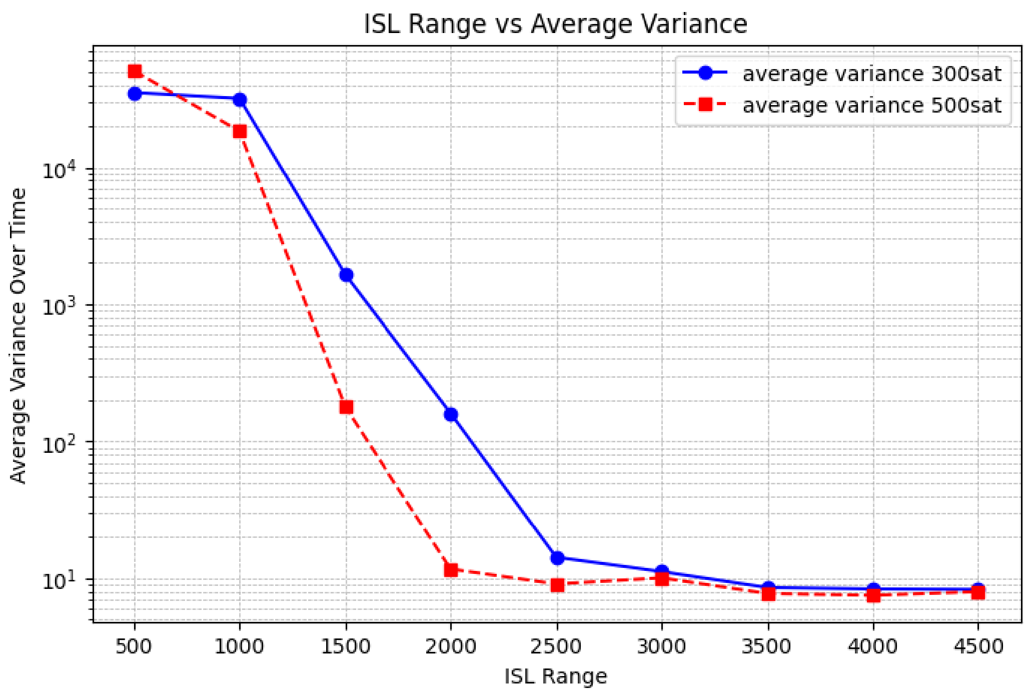

Figure 5.5: Average variance over time for different numbers of satellites and ISL range combination

horizon, and the result is shown in Figure 5.5. The results show a trend of a decrease in the average variance as the ISL range increases for both 300 and 500 satellites cases. The downward trend stopped once the ISL range crossed a certain threshold, then transitioned into a stable state.

The simulations reveal some useful facts for future constellation design. First, the consensus algorithm is effective in synchronizing all the clocks for the satellites. Second, for a small number of LEO satellites, within the current ISL communication capability, a connected network can be formed. Lastly, the connectivity of the graph increased as the ISL range increased.

Chapter 6

CONCLUSIONS

Over the past few decades, there has been great development of positioning, time, and navigation (PNT) satellite constellations. From the earliest GPS system (USA), to more recent GLONASS (Russia) and Beidou (China), many countries and entities have put tremendous effort into developing these systems. With the surge of new space technology, such as inter-satellite link, cubesats, and higher requirements for accuracy, robustness, and security, designing the next generation of PNT constellations has brought great interest to various communities. The timing system is one of the most important services provided by the PNT constellations, and the synchronization of the clocks onboard the PNT satellites is the key to ensuring the function of the time systems. Traditional time synchronization relies on the communication between the satellite and the ground stations, which is easily disturbed by many factors. Some more recent missions explore using the inter-satellite link for time transfer and synchronization. The current work aims to research the important aspects of the time system design for the PNT constellations incorporating the inter-satellite links and graph theory.

This thesis first investigates the stable time scale generation for a group of clocks, which aims to combine the advantages of different types of clocks and enhance robustness of the clock network. In this part, the clocks are model as a linear time-invariant system with states are clock bias and frequency drift. Different types clocks are distinguish by different process noise covariance matrix. The clock ensemble generation relies on a Kalman filter estimating the clock bias of all the clocks in the group and then compute a weighted sum of them, which also call implicit ensemble mean (IEM). The measurement for the Kalman filter is the clock difference between each other. The clock difference between satellite s can be determined by using time-transfer when ISLs are available. As the implicit ensemble mean is a vertual reference, another Kalman filter and control algorithm are needed to realize this reference, feedback control algorithm has been used in this research. The simulation results showed the IEM provides higher stability than any single clocks within the group, ables to inhereit the long term stability of the rubidium atomic clock and short term stability of the OCXO clocks, and the control algorithm demonstrate its effectiveness to steer a clock to track this reference.

The other problem being investigate by this thesis is the time synchronization problem. The first approach is to synchronize with the existing PNT constellations such as GPS. This avenue utilize the psuedorange measurement from the GPS satellites. A nonlinear least square method and a Kalman filter combing the clock dynamics and orbital dynamics were investigated. Both methods were simulated on a low earth orbit satellite and demonstrated effectiveness on tracking the bias between the satellite clock and GPS time. It is also observed that the nonlinear least square provides a better acuracy.

On the other hand, a Proportional-Integrate (PI) consensus algorithm was investigated to achieve synchronization between a satellite network. This approach allows for synchronization without the ground sation or current PNT systems, which provides higher robustness. The PI consensus algorithm considers a simpler clock reading dynamics derived from the two-state clock dynamics, while the control input is rely on the neighbor's clock reading, which can be access in the existence of the ISLs. The convergence of the consensus algorithm depends on the graph formed by the satellites and their links. In this work, the link establishment is constraint by the distance. Numerical simulation were done for different combination of number of LEO satellites and range distance. The results demonstrated that this consensus algorithm will converge with only a small subset of satellites from the starlink constellation within the ISL range limit. In addition, the simulation showed the performance of consenus reached upper bound for some threshold ISL distance, which implies that the graph created by the satellites and ISLs becomes a connected graph after reaching the communication range threshold. This result will be useful for future PNT cosntellation network design.

In summary, by intergrating the inter-satellite links, this work explores how time scale genration and clock synchronization can be achieved for satellite constellations.

6.1 Future Efforts

This research focuses on two fundamental aspects of the timing systems in the PNT satellite constellations. The following directions worth further exploration:

- Synchronization considering relativistic effect: As the satellites are moving around the Earth at high speed, it is necessary to consider the physical phenomena such as the relativistic effects. For Earth-based navigation systems such as GPS, this effect has been investigated. However, for future deep space exploration missions such as Lunar PNT or Mars PNT, the relativistic effect due to other celestial bodies must also be considered.

- Incorporating low-cost clocks: The current GNSS systems, like GPS, are usually equipped with multiple atomic clocks, which provide high stability, but at a high cost at the same time, which limits the scalability. For mega constellations, the low-cost clocks must be considered. These types of clocks are easy to drift due to temperature, radiation, and many other factors. Therefore, new algorithms for real-time calibration and synchronization are worth researching.

- Network design for PNT satellite constellations: The consensus algorithm's convergence relies on the communication graph created by the satellites and inter-satellite links. In this work, the only communication constraint considered was the distance. However, the link establishment is also constrained by the attitude of the satellite, and the number of links is also constrained. These constraints must be incorporated and will raise new geometry design problems for the satellite constellation.

BIBLIOGRAPHY

[1] Christian Trainotti, Tobias D. Schmidt, and Johann Furthner. Simulating the realization of a mixed clock ensemble. In *2019 Joint Conference of the IEEE International Frequency Control Symposium and European Frequency and Time Forum (EFTF/IFC)*, pages 1–11, 2019.

[2] Bradford W. Parkinson, Y.T. Jade Morton, Frank van Diggelen, and James J. Spilker Jr. *Introduction, Early History, and Assuring PNT (PTA)*, chapter 1, pages 1–42. John Wiley & Sons, Ltd, 2020.

[3] John W. Betz. *Fundamentals of Satellite-Based Navigation and Timing*, chapter 2, pages 43–64. John Wiley & Sons, Ltd, 2020.

[4] Rakesh Verma and Manu Kotwal. Global positioning system (GPS): Evolution, history, and diverse applications. *International Journal of Multidisciplinary Research Review*, 6:646–652, 04 2025.

[5] Peter H. Dana. Global positioning system (GPS) time dissemination for real-time applications. *Real-time Systems*, 12(1):9–40, 1997.

[6] W. Lewandowski, J. Azoubib, and W.J. Klepczynski. GPS: primary tool for time transfer. *Proceedings of the IEEE*, 87(1):163–172, 1999.

[7] W. Lewandowski and E.F. Arias. GNSS times and UTC. *Metrologia*, 48(4):S219–S224, 2011.

[8] Byron E. Blair and United States. National Bureau of Standards. *Time and frequency: theory and fundamentals*. NBS monograph ; 140. U.S. National Bureau of Standards, Gaithersburg, Maryland, 1974.

[9] James Camparo. The rubidium atomic clock and basic research. *Phys. Today*, 60(11):33–39, November 2007.

[10] Bernd Eissfeller, Thomas Pany, Dominik Dötterböck, and Roger Förstner. A comparative study of LEO-PNT systems and concepts. In *Proceedings of the ION 2024 Pacific PNT meeting*, pages 758–782, 2024.

[11] Winfried Stock, Robert T. Schwarz, Christian A. Hofmann, and Andreas Knopp. Survey on opportunistic PNT with signals from LEO communication satellites. *IEEE Communications Surveys and Tutorials*, 27(1):77–107, 2025.

[12] F. S. Prol, R. Morales Ferre, Z. Saleem, P. Valisuo, C. Pinell, E. S. Lohan, M. Elsanhoury, M. Elmusrati, S. Islam, K. Celikbilek, K. Selvan, J. Yliaho, K. Rutledge, A. Ojala, L. Ferranti, J. Praks, M. Z. H. Bhuiyan, S. Kaasalainen, and H. Kuusniemi. Position, navigation, and timing (PNT) through low earth orbit (LEO) satellites: A survey on current status, challenges, and opportunities. *IEEE Access*, 10:83971–84002, 2022.

[13] G. Panfilo and F. Arias. The Coordinated Universal Time (UTC). *Metrologia*, 56(4):42001–, 2019.

[14] Lorenzo Galleani. A tutorial on the two-state model of the atomic clock noise. *Metrologia*, 45(6):S175–S182, 2008.

[15] André J Van Dierendonck and J. B. McGraw. Relationship between Allan variances and Kalman filter parameters. In *Proceedings of the 16th Annual Precise Time and Time Interval Systems and Applications Meeting*, pages 273–293, 1984.

[16] Norman F. Ramsey. History of atomic clocks. *Journal of Research of the National Bureau of Standards*, 88(5):301, 1983.

[17] Thejesh N. Bandi. A comprehensive overview of atomic clocks and their applications. *BEMS Reports*, 9(1):1–10, 2023.

[18] David W Allan and James A Barnes. A modified Allan variance with increased oscillator characterization ability. In *Proceedings of the 35th Annual Frequency Control Symposium*, volume 5, pages 470–475, 1981.

[19] D.W. Allan. Statistics of atomic frequency standards. *Proceedings of the IEEE*, 54(2):221–230, 1966.

[20] D. B. Sullivan, United States. National Bureau of Standards., David W. Allan, David A. Howe, and F. L. Walls. *Characterization of Clocks and Oscillators*. NIST Technical Note ; 1337. U.S. Dept. of Commerce, National Institute of Standards and Technology, Gaithersburg, MD, 1990.

[21] R. E. Kalman. A new approach to linear filtering and prediction problems. *Journal of Basic Engineering*, 82(1):35–45, 1960.

[22] Youngjoo Kim and Hyochoong Bang. Introduction to Kalman filter and its applications. In *Introduction and implementations of the Kalman filter*. IntechOpen, 2018.

[23] John L. Crassidis and John L. Junkins. *Optimal Estimation of Dynamic Systems*. Chapman & Hall/CRC applied mathematics and nonlinear science series. Chapman & Hall/CRC, Boca Raton, 1 edition, 2004.

[24] S. F. Schmidt. The Kalman filter - its recognition and development for aerospace applications. *Journal of Guidance and Control*, 4(1):4–7, 1981.

[25] Lorenzo Galleani and Patrizia Tavella. Time and the Kalman filter. *IEEE Control Systems Magazine*, 30(2):44–65, 2010.

[26] Judah Levine. A review of time and frequency transfer methods. *Metrologia*, 45(6):S162–S174, 2008.

[27] David W. Allan and Marc Abbott Weiss. Accurate time and frequency transfer during common-view of a GPS satellite. In *34th Annual Symposium on Frequency Control*, pages 334–346. IEEE, 1980.

[28] David L. Mills. Internet time synchronization: the network time protocol. *IEEE Transactions on Communications*, 39(10):1482–1493, 2002.

[29] Gianna Panfilo and E. Felicitas Arias. Algorithms for international atomic time. *IEEE Transactions on Ultrasonics, Ferroelectrics, and Frequency Control*, 57(1):140–150, 2010.

[30] D.W. Hanson. Fundamentals of two-way time transfers by satellite. In *Proceedings of the 43rd Annual Symposium on Frequency Control*, pages 174–178, 1989.

[31] Daniel Zelazo, Mehran Mesbahi, and Mohamed-Ali Belabbas. Graph theory in systems and controls. In *2018 IEEE Conference on Decision and Control (CDC)*, pages 6168–6179, 2018.

[32] Mehran Mesbahi and Magnus Egerstedt. *Graph Theoretic Methods in Multiagent Networks*. Princeton series in applied mathematics. Princeton University Press, Princeton, 2010.

[33] Wei Ren and Randal W. Beard. *Distributed Consensus in Multi-Vehicle Cooperative Control: Theory and Applications*. Communications and control engineering. Springer, London, 2008.

[34] Francesco Bullo, Jorge Cortés, and Sonia Martínez. *Distributed Control of Robotic Networks: A Mathematical Approach to Motion Coordination Algorithms*. Princeton series in applied mathematics. Princeton University Press, Princeton, 2009.

[35] Reza Olfati-Saber, Joanna Fax, and Richard M. Murray. Consensus and cooperation in networked multi-agent systems. *Proceedings of the IEEE*, 95:215–233, 2007.

[36] Wei Ren and Randal W. Beard. Consensus seeking in multiagent systems under dynamically changing interaction topologies. *IEEE Transactions on Automatic Control*, 50:655–661, 2005.

[37] James R. Wright. GPS composite clock analysis. *International Journal of Navigation and Observation*, 2008(1):261384, 2008.

[38] Kenneth R. Brown. The theory of the GPS composite clock. *Ionics*, 4:223–242, 1991.

[39] Marion Gödel, Tobias D. Schmidt, and Johann Furthner. Kalman filter approaches for a mixed clock ensemble. In *2017 Joint Conference of the European Frequency and Time Forum and IEEE International Frequency Control Symposium (EFTF/IFCS)*, pages 666–672, 2017.

[40] Yuyue Yan, Takahiro Kawaguchi, Yuichiro Yano, Yuko Hanado, and Takayuki Ishizaki. Structured Kalman filter for time scale generation in atomic clock ensembles. *IEEE Control Systems Letters*, 8:187–192, 2024.

[41] Tobias D. Schmidt, Christian Trainotti, Jacques Isoard, Gabriele Giorgi, Johann Furthner, and Christoph Günther. Composite clock algorithms for system time in global navigation satellite systems. In *Proceedings of the 31st International Technical Meeting of the Satellite Division of the Institute of Navigation (ION GNSS+ 2018)*, pages 963–967, Miami, Florida, September 2018.

[42] Charles A. Greenhall. A review of reduced Kalman filters for clock ensembles. *IEEE Transactions on Ultrasonics, Ferroelectrics, and Frequency Control*, 59(3):491–496, 2012.

[43] Mladen Zrinjski, Đuro Barković, and Kristina Matika. Development and modernization of GNSS. *Geodetski List*, 73 (96):45–65, 03 2019.

[44] Yuanxi Yang, Weiguang Gao, Shuren Guo, Yue Mao, and Yufei Yang. Introduction to BeiDou-3 navigation satellite system. *NAVIGATION*, 66(1):7–18, 2019.

[45] Pratap Misra and Per Enge. *Global Positioning System: Signals, Measurements, and Performance*. Ganga-Jamuna Press, Lincoln, Mass, 2nd edition, 2006.

[46] F. Landis Markley and John L. Crassidis. *Fundamentals of Spacecraft Attitude Determination and Control*. Space technology library ; 33. Springer, New York, 2014.

[47] Howard D. Curtis. *Orbital Mechanics for Engineering Students.* Butterworth-Heinemann, Oxford, 2019.

[48] CelesTrak. Celestrak, 2025. Available at `https://celestrak.org/`. Accessed: 2025-01-15.

[49] Brandon Rhodes. Skyfield: Astronomy for python. `https://rhodesmill.org/skyfield/`, 2019. Accessed: 2025-01-15.

[50] James Bradbury, Roy Frostig, Peter Hawkins, Matthew James Johnson, Yash Katariya, Chris Leary, Dougal Maclaurin, George Necula, Adam Paszke, Jake VanderPlas, Skye Wanderman-Milne, and Qiao Zhang. JAX: composable transformations of Python+NumPy programs, 2018.

[51] Ron Hatch. The synergism of GPS code and carrier measurements. In *International geodetic symposium on satellite doppler positioning*, volume 2, pages 1213–1231, 1983.

[52] Heena Arora and Rakesh Goyal. A review on inter-satellite link in inter-satellite optical wireless communication. *Journal of Optical Communications*, 38(1):63–67, 2017.

[53] Gayatri Tiwari and Ram Chandra Singh Chauhan. A review on inter-satellite links free space optical communication. *Indian Journal of Science and Technology*, 13(6):712–724, 2020.

[54] R. Carli, A. Chiuso, L. Schenato, and S. Zampieri. A PI consensus controller for networked clocks synchronization. *IFAC Proceedings Volumes*, 41(2):10289–10294, 2008.

Appendix A

GPS SATELLITE GEOMETRY AND DILUTION OF PRECISION

The GPS geometry matrix in estimating the position and clock bias is defined as

$$G = \begin{bmatrix} -(\mathbf{1}^1)^T & 1 \\ -(\mathbf{1}^2)^T & 1 \\ \vdots & \\ -(\mathbf{1}^K)^T & 1 \end{bmatrix} \tag{A.1}$$

Where

$$\mathbf{1}^k = \frac{x^k - \tilde{x}}{\|x^k - \tilde{x}\|} \tag{A.2}$$

is the normalized line-of-sight vector, and x^k and $\tilde{x}$ represent the positions of the GPS satellite and the receiver, respectively. The quality of the estimation from the Nonlinear least square method can be characterized by the geometry matrix G.

Defining $\Delta x = x - \tilde{x}$ and $\Delta b = b - \tilde{b}$, where x and b are the true position and clock bias, and $\tilde{x}$ and $\tilde{b}$ are the estimated position and bias. Assuming the pseudorange measurements are unbiased and denote the error variance of the pseudorange measurement as σ^2. The covariance of the estimation error can be computed as

$$\mathbf{cov}(\begin{bmatrix} \Delta x \\ \Delta b \end{bmatrix}) = \sigma^2 (G^T G)^{-1}. \tag{A.3}$$

It can be observed that the estimation covariance is determined completely by the error variance of the pseudorange measurement and the geometry matrix G. Let $H = (G^T G)^{-1}$. The estimated error covariance in position and bias can be analyzed by the diagonal entries of H. Hence, we have

$$\sigma_x^2 = \sigma^2 H_{11}, \sigma_y^2 = \sigma^2 H_{22}, \sigma_z^2 = \sigma^2 H_{33}, \sigma_b^2 = \sigma^2 H_{44}, \tag{A.4}$$

where H_{ii} denotes the i-th entry of the H matrix and $\sigma_x^2, \sigma_y^2, \sigma_z^2$ and σ_b^2 are the error variance of the position estimate in x, y, and z coordinates and the bias, respectively.

The term **Dilution of Precision**(DOP) provides a measure on the geometry side. The position dilution of precision (PDOP), time dilution of precision (TDOP), and geometric dilution of precision (GDOP) are defined as follows,

$$\mathbf{PDOP} = \sqrt{H_{11} + H_{22} + H_{33}} \tag{A.5}$$

$$\mathbf{TDOP} = \sqrt{H_{44}} \tag{A.6}$$

$$\mathbf{GDOP} = \sqrt{H_{11} + H_{22} + H_{33} + H_{44}}. \tag{A.7}$$

Appendix B
CONVERGENCE OF CONSENSUS

Considering the agents in the network operate in the continuous consensus protocol,

$$\dot{x}_i = \sum_{j \in \mathcal{N}_i} (x_j - x_i), \tag{B.1}$$

Then the stacked state vector $x = [x_1, x_2, \ldots, x_N]^T$ will follow the dynamic

$$\dot{x} = -Lx. \tag{B.2}$$

The solution for this dynamic is then

$$x(t) = e^{-Lt}x(0). \tag{B.3}$$

where $x(0)$ corresponds to the initial condition of all agents. Given an arbitrary undirected connected graph, the eigenvalues of the Laplacian matrix satisfy $0 = \lambda_1 \leq \lambda_2 \leq \cdots \leq \lambda_N$. Denote the diagonal matrix consist of the eigenvalues of the Laplacian as

$$\Sigma = \begin{bmatrix} \lambda_1 & 0 & \ldots & 0 \\ 0 & \lambda_2 & \ldots & 0 \\ \vdots & \vdots & \ldots & \vdots \\ 0 & 0 & \ldots & \lambda_N \end{bmatrix}, \tag{B.4}$$

The eigendecomposition of the Laplacian matrix is then $L = U\Sigma U^T$ where $U = [u_1|u_2|\ldots|u_N]^T$ consists of normalized eigenvectors corresponding to the eigenvalues. The solution for the consensus dynamic can then be written as follows

$$x(t) = e^{-Lt}x_0 \tag{B.5}$$

$$= e^{-U\Sigma U^T t}x(0) \tag{B.6}$$

$$= Ue^{-\Sigma t}x(0)U^T \tag{B.7}$$

and decomposed along the eigen-axis into

$$x(t) = e^{-\lambda_1 t}(u_1^T x(0))u_1 + e^{-\lambda_2 t}(u_2^T x(0))u_2 + \cdots + e^{-\lambda_N t}(u_N^T x(0))u_N \tag{B.8}$$

According to the assumption of the eigenvalues of the Laplacian for a connected graph, all the individual terms go to 0 since $0 < \lambda_2 < \cdots < \lambda_N$, and $x(t)$ converges to $u_1^T x(0) u_1$ since $\lambda_1 = 0$. The eigenvector corresponding to λ_1 is $u_1 = [\frac{1}{\sqrt{n}}, \ldots, \frac{1}{\sqrt{n}}]^T$, therefore, the consensus dynamic will lead all the agents to the value

$$x(t) \to \frac{\mathbf{1}^T x(0)}{n}\mathbf{1}. \tag{B.9}$$

as $t \to \infty$.

The discrete-time version of the consensus protocol is the following:

$$x_i(k+1) = x_i(k) + \alpha \sum_{j \in \mathcal{N}_i} (x_j(k) - x_i(k)), \tag{B.10}$$

where α is a coefficient that satisfies $0 < \alpha < \frac{1}{\Delta}$ with Δ being the maximum degree of the graph. The stacked state dynamic is then

$$x(k+1) = (I - \alpha L)x(k). \tag{B.11}$$

To show the convergence of the discrete-time consensus protocol under the assumption that a graph is connected, a similar approach to the continuous version can be taken. Perform the eigendecomposition of the system, and define the transformed state vector $\tilde{x}(k) = U^T x(k)$, then obtain:

$$x(k+1) = U(I - \alpha\Sigma)U^T x(k) = \tilde{x}(k+1) = (I - \alpha\Sigma)\tilde{x}(k). \tag{B.12}$$

Since the identity matrix and Σ are diagonal matrices, this allows for analyzing the system on each coordinate, with each coordinate being

$$\tilde{x}_i(k+1) = (1 - \alpha\lambda_i)\tilde{x}_i(k). \tag{B.13}$$

For the first coordinate with $\lambda_1 = 0$, it have

$$\tilde{x}_1(k+1) = \tilde{x}_1(k) \Rightarrow \tilde{x}_1(k) = \tilde{x}_1(0). \tag{B.14}$$

For the coordinates other than the first coordinate, the condition for α ensures that $0 < 1 - \alpha\lambda < 1$, and so $\lim_{k\to\infty}(1 - \alpha\lambda_i)^k = 0$. Hence,

$$\tilde{x}_i(k+1) = (1 - \alpha\lambda_i)\tilde{x}_i(k) \Rightarrow \tilde{x}_i(k) = (1 - \alpha\lambda_i)^k \tilde{x}_i(0) = 0. \tag{B.15}$$

Stacking all the results from above, as $k \to \infty$, the transformed state vector becomes

$$\tilde{x}(k) = [\tilde{x}_1(0), 0, \dots, 0]^T. \tag{B.16}$$

Performing the inverse transform, and using the fact that the first eigenvector for the Laplacian is $u_1 = [\frac{1}{\sqrt{n}}, \dots, \frac{1}{\sqrt{n}}]^T$, then

$$\begin{aligned} x(k) = U\tilde{x}(k) &= u_1(u_1^T x(0)) && \text{(B.17)} \\ &= \frac{\mathbf{1}^T x(0)}{n}\mathbf{1} && \text{(B.18)} \end{aligned}$$

as $k \to \infty$.